# Computing Symmetry Sets from 2D Shapes

**Arjan Kuijper**

**IT University Technical Report Series** **TR-2003-36**

**ISSN 1600–6100** **October 2003**

**ISSN 1600–6100**

**ISBN 87-7949-049-2**

**Copies may be obtained by contacting:**

**IT University of Copenhagen**
**Glentevej 67**
**DK-2400 Copenhagen NV**
**Denmark**

| | |
|---|---|
| **Telephone:** | **+45 38 16 88 88** |
| **Telefax:** | **+45 38 16 88 99** |
| **Web** | **`www.itu.dk`** |

# Contents

**Abstract**

*Many attempts have been made to represent families of 2D shapes in a simpler way. These approaches lead to so-called structures as the Symmetry Set ($\mathcal{SS}$) and a subset of it, the Medial Axes ($\mathcal{MA}$). While the latter is commonly used, the former is still in the mathematical research stage. One reason for this is that in contrast to the $\mathcal{SS}$, the $\mathcal{MA}$ can be computed efficiently and fastly, and yields one connected component for a closed shape. A drawback of the $\mathcal{MA}$ representation is its graph-structure that makes comparison with the $\mathcal{MA}$ of another shape difficult and time-consuming.*

*In this paper a novel method to represent the $\mathcal{SS}$ as a string is presented. This structure allows faster and simpler query algorithms for comparison and database applications. Second, new ways to visualize these sets are presented. They use the distances from the shape to the set as extra dimension as well as the so-called pre-Symmetry Set (pre-$\mathcal{SS}$). Information revealed by these representations can be used to calculate the novel representation structure that is based on the $\mathcal{SS}$ and the shape's evolute.*

*Example shapes are shown and their datastructures derived. They show the stability and robustness of the latter, compared to the $\mathcal{MA}$.*

# 1 Introduction

In 2D shape analysis the simplification of shapes into a skeleton-like structure is widely investigated. The Medial Axis ($\mathcal{MA}$) skeleton is commonly used, since it can be calculated in a fast and robust way. Many results on simplification, reconstruction and database search are reported, see e.g. [3, 7, 11, 12, 21, 24, 27, 28, 29, 33, 31, 35, 32, 34, 36, 39, 38]. The $\mathcal{MA}$ is a member of a larger family, the Symmetry Set ($\mathcal{SS}$), exhibiting nice mathematical properties, but more difficult to compute than the $\mathcal{MA}$. It also yields distinct branches, i.e. unconnected "skeleton" parts, which makes it hard to fit into a graph structure (like the $\mathcal{MA}$) for representation.

In section 2 the definitions of these sets and related properties are given. They result for example in so-called Shock Graphs, a $\mathcal{MA}$ skeleton, augmented with information of the distance from the boundary (the distance function) at which special skeletonpoints occurs.

Section 3 is concerned with the computation of the $\mathcal{MA}$ and the $\mathcal{SS}$. The simpleness of the $\mathcal{MA}$ allows a fast and efficient computation using partial derivative equations (PDE's). The complexity of the $\mathcal{SS}$ prohibits these methods, as well as modifications of them. Alternatively, geometrical methods must be used. The complexity of the algorithms needed depend on the number of points evaluated on the shape.

While the 2D visualization of the $\mathcal{MA}$ skeleton is unambiguous, the $\mathcal{SS}$ may give rise to intersecting curves that occur due to its very nature. Therefore, representation of the $\mathcal{SS}$ is not trivial and in section 4 issues regarding representation are discussed. Extra information about the shape and its $\mathcal{SS}$ is given by the evolute, where all its non-differential points relate to endpoints of the $\mathcal{SS}$. With the need for augmenting the skeleton with the distance function, the need for a representation in a space with an extra dimension (viz. the distance) is evident. This space also visualizes why new branches of the skeleton may suddenly appear when the shape is slightly perturbed. These branches are parts of the Symmetry Set that 'suddenly' become part of the Medial Axis. The shape in the parameterized space can be studied using the so-called pre-Symmetry Set (pre-$\mathcal{SS}$). This set allows one to extract special points on the Symmetry Set relatively easy.

To overcome the complexity of the $\mathcal{SS}$ with respect to the $\mathcal{MA}$, we introduce in section 5 a datastructure containing both the symmetry set and the evolute of the shape, resulting in a representational datastructure that is less complex and more robust than the $\mathcal{MA}$-based structures.

Examples are given on a convex shape, showing the stability and robustness of the new datastructure, in section 6 and a concave shape in section 7, followed by the conclusions in section 8 and two appendices concerning some numerical details and new open questions related to the results obtained.

# 2 Shapes

In this section we give the necessary background regarding properties of shapes, the Medial Axis, the Symmetry Set, labeling points on these sets and give an example to clarify the definitions.

Let $\mathcal{S}(x(t), y(t))$ denote a closed 2D shape and $(.)_t = \frac{\partial(.)}{\partial t}$, then $\mathcal{N}(t) = (-y_t, x_t)/\sqrt{x_t^2 + y_t^2}$ denotes its unit normal vector, and $\kappa(t) = (x_t y_{tt} - y_t x_{tt})/\sqrt{x_t^2 + y_t^2}^3$ is its curvature. The evolute $\mathcal{E}(t)$ is given by the

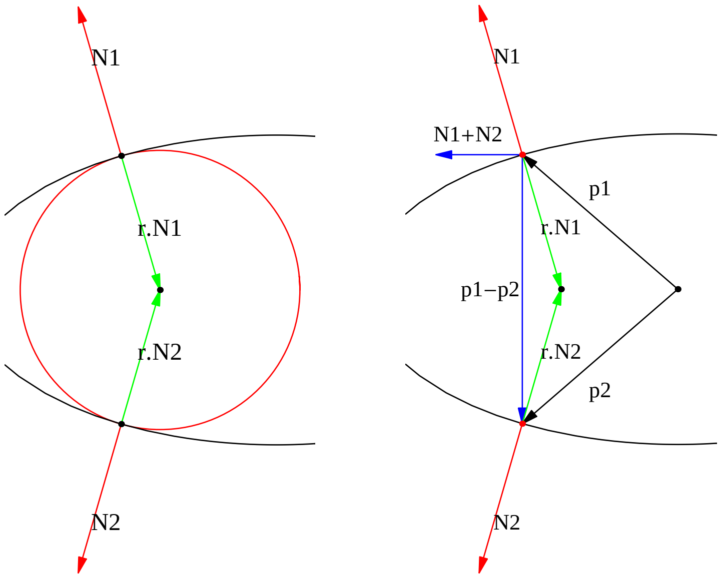


Figure 1: Deriving the Medial Axis geometrically. See text for details.

set $\mathcal{S} + \mathcal{N}/\kappa$. Note that as $\kappa$ can traverse through zero, the evolute moves "through" (minus) infinity. This occurs by definition only for concave shapes. An alternative representation can be given implicitly: $\mathcal{S}(x, y) = \{(x, y)|L(x, y) = 0\}$ for some function $L(x, y)$. Then the following formulae can be derived for $\mathcal{N}(x, y)$ and $\kappa(x, y)$:

$$\mathcal{N}(x,y) = \left( \frac{L_x}{\sqrt{L_x^2 + L_y^2}}, \frac{L_y}{\sqrt{L_x^2 + L_y^2}} \right)$$

and

$$\kappa(x,y) = -\frac{L_x^2 L_{yy} - 2L_x L_y L_{xy} + L_y^2 L_{xx}}{\sqrt{L_x^2 + L_y^2}^{\,3}}$$

Although the curve is smooth and differentiable, the evolute contains non-smooth and non-differentiable points, viz. those where the curvature is zero or takes a local extremum, respectively.

#### 2.0.1 Example

The ellipse $\mathcal{S}(x(t), y(t)) = (2\cos(t), \sin(t))$ has normalvectors $\mathcal{N}(t) = -(\cos(t), 2\sin(t))(\cos^2(t)+4\sin^2(t))^{-1/2}$ and curvature $\kappa = 2(\cos^2(t)+4\sin^2(t))^{-3/2}$, with the extremal values 2, for $t = 0$ and $t = \pi$ and $1/4$ for $t = \pi/2$ and $t = 3\pi/2$,

In $(x, t)$ coordinates this ellipse can be defined by $L(x, y) = x^2 + 4y^2 - 4$, with $\mathcal{N}(x, y) = (x, 4y)(x^2 + 16y^2)^{-1/2}$, and $\kappa(x, y) = -4(x^2 + 4y^2)(x^2 + 16y^2)^{-3/2}$. The extremal values of $\kappa$ are 2, for $(x, y) = (\pm 2, 0)$, and $1/4$ for $(x, y) = (0, \pm 1)$. The evolute consists of four parts, joined at cusps at the locations $(0, \pm 3)$ and $(\pm 3/2, 0)$. For a drawing, see Figure 4.

## 2.1 Medial Axis

The Medial Axis ($\mathcal{MA}$) is defined as the closure of the set of centers of circles within the shape that are tangent to the shape at at least two points and that contain no other tangent circles: they are so-called maximal circles.

To calculate this set from above definition, the following procedure can be used, see Figure 1: Let a circle with unknown location be tangent to the shape at two points (left). Then its center can be found by using the

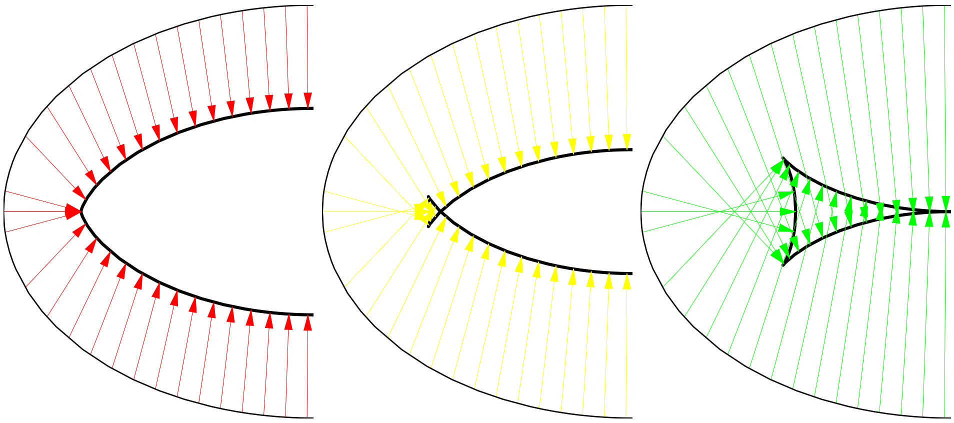

Figure 2: Deriving the Medial Axis from the intersections of the distance function.

**normalvectors at these points: it is located at the position of each point minus the radius of the circle times the normal vector at each point.**

**To find these two points, the location of the center and the radius, do the following: Given two vectors $p_i$ and $p_j$ (Figure 1, right, with $i = 1$ and $j = 2$) pointing at two locations at the shape, construct the difference vector $p_i - p_j$. Given the two unit normal vectors $N_i$ and $N_j$ at these locations, construct the vector $N_i + N_j$. If the two constructed vectors are non-zero and perpendicular,**

$$(p_i - p_j).(N_i \pm N_j) = 0, \tag{1}$$

**the two locations give rise to a tangent circle. The radius $r$ and the center of the circle are given by**

$$p_i - rN_i = p_j \pm rN_j \tag{2}$$

**and one only has to make sure that the center of the circle lies within the shape and that the circle is maximal.**

#### 2.1.1 Example

**The aforementioned ellipse $L(x, y) = x^2 + 4y^2 - 4$ has a $\mathcal{MA}$ formed by a straight line along the $x$-axis with its endpoints at the cusps of the evolute within the shape: $(\pm 3/2, 0)$: there the smallest circles with radius $1/2$ fit, while the biggest circle with radius $1$ is located at the origin.**

### 2.2 Distance function

**As an alternative and fast method, one can also trace all unit normal vectors at the shape simultaneously and continuously, and locate the points where different vectors intersect each other. The unit normal vectors are multiplied with a (negative) constant $\alpha$, and the shape at the new location $\mathcal{S}_\alpha = \mathcal{S} + \alpha\mathcal{N}$ is calculated. This shape has distance $\alpha$ from the original shape. The $\mathcal{MA}$ points are then given by the intersection points of the new locations of the shape: at these positions the new shape has a minimal distance to a least two different locations at the original shape, see Figure 2. Note that the swallowtails in the second and third image are imaginary in this viewpoint, since they will (eventually) only constitute circles that are not maximal. The endpoints of the $\mathcal{MA}$ are given by the non-differential points of the evolute: if $\alpha = \kappa$ the first (final) intersection takes place, see the left image of Figure 2.**

**Consequently, the $\mathcal{MA}$ arises as the discontinuities of the 2D manifold in 3D spanned by $(\mathcal{S}_\alpha, \alpha)$. This can easily be visualized as a mountainlandscape. The discontinuities appear as ridges and ravines, i.e. elongated, connected curved structures. Isolated points are non-generic, an infinitesimal small perturbation of the shape would either remove them or transform them into a connected structure.**

#### 2.2.1 Example

The aforementioned ellipse $L(x, y) = x^2 + 4y^2 - 4$ has a $\mathcal{MA}$ formed by a straight line along the $x$-axis with its endpoints at the cusps of the evolute within the shape: $(\pm 3/2, 0)$. These two points are obtained from the original shape points $(x, y) = (\pm 2, 0)$, i.e. at the 3D locations $(x, y, \alpha) = [\pm 3/2, 0, -1/2)$. For decreasing $\alpha$ two ravine segments appear that merge at $(x, y, \alpha) = (0, 0, -1)$.

#### 2.2.2 Augmentation

It is known that the $\mathcal{MA}$ in itself carries insufficient information for representing and reconstruction a shape, since different shapes can yield the same $\mathcal{MA}$, see [15]. Therefore additional information can be added to the $\mathcal{MA}$ and used, as proposed by various authors as described below. Based on the behaviour of the radii one can distinguish between special points along the $\mathcal{MA}$, as well as impose vectors on the $\mathcal{MA}$ denoting increasing or decreasing radiusflow.

#### 2.2.3 Shock Graphs

The special points on the $\mathcal{MA}$ defined by Sidiqqi et al. in their shock graph method [32, 34] results in four types describing the changes of the radius:

1. protrusion: ordinary points on the $\mathcal{MA}$ where the radius is increasing.
2. necks of the shape, the radius minimum on the parameterized $\mathcal{MA}$.
3. bends of the shape: maxwell set of the points on the $\mathcal{MA}$ (no change in radius for a while).
4. an annihilation point, or a maximum of the radius.

Subclassification is applicable when regarding the radiusflow. Sebastian et al., see e.g. [28, 29], and Pelillo et al. [26], applied shock graphs to searching in large databases. Tek and Kimia [38, 37, 39] smooth the shape by editing the medial axis based on removing shocks.

#### 2.2.4 R-skeletons

In the work of Kunii et al. [24], R-skeleton are considered, being the set of all singular points of the distance map, which is a generalization of the $\mathcal{MA}$, since all circles inside the shape are considered. They build a hierarchical structure based on Gaussian or wavelet smoothing in order to smooth the obtained structure. The R-skeleton is either ridge or ravine, including special locations where ridges and/or ravines meet, start or end. Belyaev et al. [3] describe the relation between the evolute and the skeleton: if a cusp moves through a skeleton, sometimes a new branch of the skeleton appears. Hisada et al. [21] approach the skeleton by the Voroni diagram with quite some heuristic assumptions, again finding the ridges and ravines.

#### 2.2.5 Reconstruction

The $\mathcal{MA}$ together with the flow of radius function, as well as information in the special points, are sufficient to reconstruct the shape, as shown by Giblin and Kimia [13, 15].

### 2.3 Symmetry Sets

The restriction in the $\mathcal{MA}$ regarding maximal circles inside the shape only may seem an unnecessarily one. If it is omitted, the Symmetry Set is obtained: The Symmetry Set $\mathcal{SS}$ is defined as the closure of the set of centers of circles that are tangent to the shape at least two points [8, 10, 14, 13, 16, 15]. Obviously, the $\mathcal{MA}$ and the R-skeleton are a subset of the $\mathcal{SS}$ [13, 15]. To find the $\mathcal{SS}$, the same procedure given in the previous section can be used.

This is illustrated in Figure 3. Given the two points $p_1$ and $p_2$, the same point is found as in the $\mathcal{MA}$ case. This time, also $p_1$ and $p_4$ and their normals satisfy the conditions given by Eqs. (1-2) with radius $s$ and a center of the circle outside the shape. So indeed extra points are found.

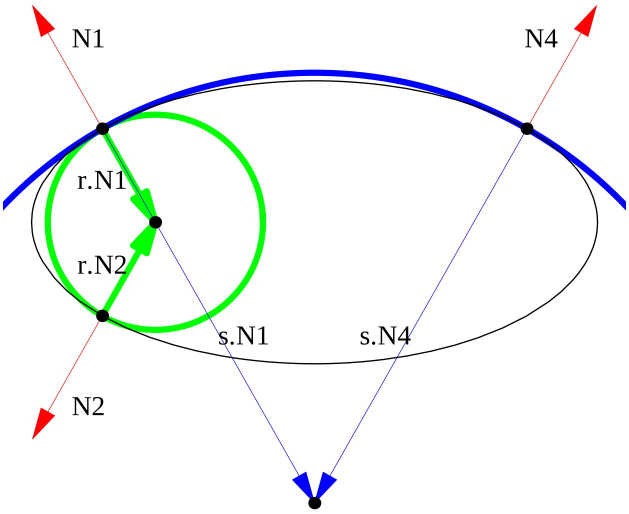


Figure 3: Deriving the Symmetry Set (right). See text for details.

### 2.3.1 Example

**The aforementioned ellipse $L(x, y) = x^2 + 4y^2 - 4$ has a $\mathcal{SS}$ formed by a straight line along the $x$-axis with its endpoints at the cusps of the evolute within the shape: $(\pm 3/2, 0)$, the $\mathcal{MA}$, and a straight line along the $y$-axis with its endpoints at the cusps of the evolute outside the shape: $(0, \pm 3)$, as shown in Figure 4.**

## 2.4 Classification of Points on the Symmetry Set

**It has been shown by Bruce et al. [10] that only five distict types of points can occur for the $\mathcal{SS}$, and by Giblin et al. [14, 13, 16, 15] that they are inherited by the $\mathcal{MA}$. These five types are:**

- **An $A_1^2$ point: the "common" midpoint of a circle tangent at two distinct points of the shape.**
- **An $A_1A_2$ point: the midpoint of a circle tangent at two distinct points of the shape but located at the evolute.**
- **An $A_1^2A_1^2$ point: the midpoint of two circles tangent at two pairs of distinct points of the shape with different radii.**
- **An $A_1^3$ point: the midpoint of one circle tangent at three distinct points of the shape.**
- **An $A_3$ point: the midpoint of a circle located at the evolute and tangent at the point of the shape with the local extremal curvature.**

### 2.4.1 Example

**The aforementioned ellipse $L(x, y) = x^2 + 4y^2 - 4$ has $A_3$ points at the four endpoints of the $\mathcal{SS}$ - the cusps of the evolute - at $(0, \pm 3)$ and $(\pm 3/2, 0)$, and an $A_1^2A_1^2$ point at the origin, where both lines cross.**

## 2.5 Properties of the Symmetry Set

**Since the $\mathcal{SS}$ is defined locally, global properties of it are not widely investigated and difficult to derive. Banchoff and Giblin [2] have proven an invariant to hold for the number of $A_3$ , $A_1A_2$, and $A_1^3$ points, both for the**

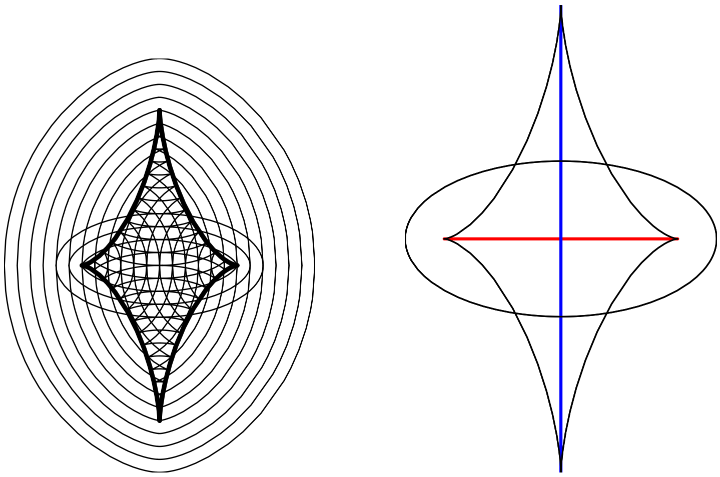

Figure 4: Left: The ellipse $\mathcal{S}$, shapes $\mathcal{S}_\alpha$ due to the distance function, and the evolute $\mathcal{E}$. Right: The ellipse $\mathcal{S}$, its evolute $\mathcal{E}$ and its $\mathcal{MA}$ (horizontal line) and $\mathcal{SS}$ (both lines).

**continuous case as the piecewise one. These numbers hold if the shape changes in such a way that the $\mathcal{SS}$ changes significantly. At these changes, called transitions [9], a so-called non-generic event for a static $\mathcal{SS}$ occurs, for instance the presence of a circle tangent to four points of the shape. Sometimes the number of $A_3$ , $A_1A_2$, and $A_1^3$ points changes when the $\mathcal{SS}$ goes through a transition. For the $\mathcal{MA}$ part it implies e.g. the birth of a new branch of the skeleton. A list of possible transitions, derived from [9] is given in section 5.3.**

# 3 PDE methods

**The computation of the intersections of $\mathcal{S}_\alpha = \mathcal{S} + \alpha\mathcal{N}$, as described in section 2.2, can be formalized as solving the so-called normal motion flow**

$$\frac{\partial S}{\partial t} = \mathcal{N} \tag{3}$$

**with initial condition $S(0) = \mathcal{S}$, by taking infinitesimal steps $t$: $\mathcal{S}_t - \mathcal{S} = \mathcal{S} + t\mathcal{N} - \mathcal{S} = t\mathcal{N}$, so**

$$\frac{\mathcal{S}_t - \mathcal{S}}{t} = \mathcal{N} \ ,$$

**and taking the limit for $t \to 0$ gives Eq. (3). This equation is also know as Grassfire equation, since it can be considered as describing the burning of grassland starting at $\mathcal{S}$. Solving this equation yields the 2D manifold with the $\mathcal{MA}$ as the discontinuities where non-smooth parts of the dome are 'glued' together.**

## 3.1 Level Sets

**Since most shapes are not given in a parameterized way, but as some zero-level set, e.g. the boundary of an object, the implicit representation described in section 2 is commonly used. The 2D implicit representation of Eq. (3) is given by a so-called Hamilton-Jacobi equation:**

$$\frac{\partial u}{\partial t} = \|\nabla u\| \tag{4}$$

**with initial condition that $u(x, y, 0) = \mathcal{S}$, the given shape. The solution $u(x, y, t)$ satisfies $u(\mathcal{S}, t) = 0, \forall t$. Level set methods [25, 30] are commonly used to solve this equation. Just as in the parameterized version, for small time (distance) steps the new shape at the new time is calculated. Due to numerical errors, however, the newly calculated shape does not exactly lie on the manifold prescribed by the distance function, so a reinitialization step is needed before a next time step can be taken.**

### 3.1.1 Level set methods vs. geometric methods

Recently, Gomes and Faugeras [20] pointed out that in order to overcome reinitialization problems for the more general equation

$$\frac{\partial \mathcal{S}}{\partial t} = \beta \mathcal{N}$$

with $u(S,t) = 0, \ \forall t$, and where $\beta$ is some velocity function, one should not use the Hamilton-Jacobi equation

$$\frac{\partial u}{\partial t} = \beta ||\nabla u||$$

since the solution of the latter is not the signed distance function to the solution of $S$ in the former, but use

$$\frac{\partial u}{\partial t} = \beta ||x - u \nabla u||$$

whose integral version reads

$$u(\mathcal{S} + \lambda \mathcal{N}) = \lambda, \quad \forall t$$

and the relation with the geometric method described earlier is clear.

## 3.2 Hamilton Jacobi Skeletons

The exact location of the shock graph points with PDE based methods is difficult to find, but the Hamilton Jacobi approach seems to be promising. It was proposed by Siddiqi et al. [35, 31]. Using the Grassfire equation, the $\mathcal{MA}$ is found by solving a Hamiltonian system that determines the shocks efficiently. It basically applies a vectorfield on the distance function-surface and traces the discontinuities of this vectorfield. Dimitrov et al. [12] added a homotopy preserving thinning algorithm in 2D. In [11] they are concerned with the mathematics needed for deriving the singularities, i.e. the skeleton. The divergence theorem yields zero on the distance function surface, but at the skeleton (the singularities of the surface) a non-zero value is found (cf. the winding number for singularities of images by Kalitzin [23]). The value found gives the angle between the normals of the shape at skeleton points, and something more complicated at the endpoints and the junction points. 3D applications are presented by Bouix and Siddiqi in [7]. All papers are nicely combined in [36].

## 3.3 Symmetry Sets

The next step would be to generalize the equations (3) and (4) such, that they return the symmetry set as the discontinuities of the solution.

In contrast to the $\mathcal{MA}$ method however, no PDE method for deriving the $\mathcal{SS}$ can be found. This becomes clear when recalling Figure 2. For the $\mathcal{SS}$ the swallowtails – imaginary in the $\mathcal{MA}$ viewpoint – are essential. Any PDE method, however, will remove these swallowtails. This is due to the fact that the intersection points, the skeletonpoints, are the points of convergence of the PDE method. The swallowtails, in contrary, are obtained by continuing through earlier intersection points. Forcing PDE methods to do this too, equals to forcing the PDE methods not to converge. This is obviously a contradiction to the basic idea of using PDE methods.

This idea is visible in Figure 5, where the distance function of the ellipse is shown. The ellipse shrinks as $\alpha$ decreases, yielding the $\mathcal{MA}$ as the bottom of the cup, with starting swallowtails (left). If $\alpha$ decreases further, the swallowtails become larger and form an 'inverse' cup. The topridge of this cup forms the non-$\mathcal{MA}$ part of the $\mathcal{SS}$. If $\alpha$ decreases further, this inverse cup keeps on growing, so any PDE along this surface converging at the point where the surface ends, will convergence at all – simply because it doesn't end.

### 3.3.1 Combining PDE methods

Although PDE methods on the complete manifold fail, one may try to construct sub-solutions, based on PDE methods and combine these solutions.

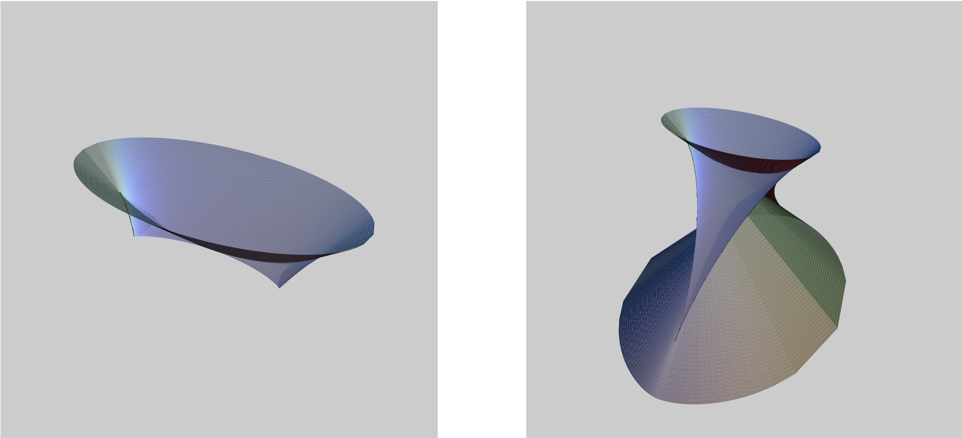

Figure 5: The manifolds for the ellipse. Left: $-1 \leq \alpha \leq 0$ Right: $-5 \leq \alpha \leq 0$.

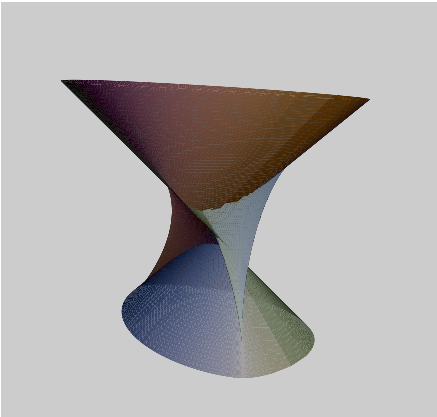

Figure 6: The manifolds for the oval, $-4 \leq \alpha \leq 0$.

**Inverting the shape** Inspired by Figure 5, one may think that a way to avoid the convergence problem is to use the PDE approach on the shape that is obtained when such a value for $\alpha$ is taken, that the shape doesn't change "significantly", i.e. topologically, anymore. For instance, the inverse cup mentioned in the previous section, doesn't change anymore when $\alpha < -5$. Using this shape $\mathcal{S}_{-5}$ as input, the complement of the $\mathcal{MA}$, viz. $\mathcal{MA}^C$, of the $\mathcal{MA}$ with respect to the $\mathcal{SS}$ will be found. Basically, this assumes that $\mathcal{SS} = \mathcal{MA} + \mathcal{MA}^C$, with $\mathcal{MA}^C$ a Medial Axis representation.

This is, however, erroneous. As an example, see Figure 6. This is the distance manifold for the shape used in section 6, a cubic oval which is a perturbation of the ellipse. Although the two main cups are visible, now also a discontinuity can be seen in the ridge-shaped branches connecting them. This is due to a selfintersection of the evolute and the consecutive extra branch of the $\mathcal{SS}$. This part is swallowtail-shaped and cannot occur in a $\mathcal{MA}$ by its definition, see e.g. [18]. For more details on this shape and its $\mathcal{SS}$, see section 6.

**Partitioning the shape** Alternatively, one can also, by investigation of Figure 2, observe that the horizontal branch of the $\mathcal{SS}$ (the $\mathcal{MA}$) is caused by the parts of the shape above and beneath the $x$-axis, and similarly for the vertical part – which is, of course, by the very definition of the sets, true. Then the shape can be divided into four parts, with endpoints the local extrema of the curvature. By applying a PDE method on the pairs that join an endpoint, one "thus" finds the $\mathcal{SS}$ branches from endpoints of the $\mathcal{SS}$ to the point where two $\mathcal{SS}$ branches are connected. In the example of the ellipse this is the origin, where each pair starting on one of the axis, meet.

This method fails too on similar arguments as in the previous section. Points on the shape contribute to multiple critical distances, independent if they are on two parts of the shape joined by an extremum of the curvature. The method proposed only takes into account two possible critical distances, thus ignoring extra points, e.g. the swallowtail structure.

#### 3.3.2 Liverpool Surface Modeling Package

The main problem with PDE methods is that they are local methods - thus enabling fast implementation. The $\mathcal{SS}$, however, is a global property of the shape. Therefore other methods - geometrically based - are needed. The Liverpool Surface Modeling Package (LSMP) is such a method. It is based on the geometrical description as mentioned in section 2.3: finding the zero-crossings of the innerproducts of vectors related to the positions and tangents of points on the parameterized shape. Instead of $(p_i - p_j).(N_i \pm N_j) = 0$, $(p_i - p_j).(T_i \pm T_j) = 0$ is taken. Given the rules for unit normals and tangents, this yields equivalent results.

#### 3.3.3 Mathematica Notebook

A major drawback of the LSMP is that it is only suited for parameterized shapes, or functions that can be parameterized. A challenging task is therefore to use the theoretical basis of the LSMP, but extending it to general shapes. Furthermore, an automatic augmentation of points on the derived $\mathcal{SS}$ is needed as well as an interactive environment allowing user- and task-dependent visualizations. This has been accomplished in the Mathematica Notebook described in Appendix A. This interactive program is used to derive the results presented in the following sections.

# 4 Representation

In this section we discuss methods to represent the $\mathcal{SS}$. Since the $\mathcal{MA}$ is a subset of the $\mathcal{SS}$, we will focus on the latter.

## 4.1 Plain in the plane

The most common way to represent the $\mathcal{MA}$ and the $\mathcal{SS}$ is just by the plotting the calculated values in the spatial coordinates as in Figure 4. For the $\mathcal{MA}$ this may seem quite trivial, since this graph is by definition the reason for its existence. For the $\mathcal{SS}$ it is less trivial, since crossings of branches of the $\mathcal{SS}$ can have different interpretation, e.g. the $A_1^2 A_1^2$ points, where two circles with different radii are involved, and $A_1^3$ points where one circles is tangent at three points. In the former case two lines intersect, in the latter case three lines intersect, so one is able to distinguish between the two cases when plotted in the plane.

## 4.2 Evolute

A way to get extra insight in the behaviour of the $\mathcal{SS}$ is by drawing its evolute, just as in Figure 4. $A_3$ points of the $\mathcal{SS}$ start (or end) at the cusp points of the evolute and $A_1 A_2$ points (the cusp points of the $\mathcal{SS}$) are located at the evolute. Furthermore, the cusps along the evolute are ordered by the parameterization of the curve.

## 4.3 Radius space

Having incorporated the radius (distance) function upon the $\mathcal{MA}$ or the $\mathcal{SS}$, one has extra information. This information can be exploited in much more detail when the radius is considered as an extra dimension. Using this dimension, the 1D curves in the 2D plane become 1D curves in 3D space. So only the discontinuities of the distance function in 3D are considered. In this 3D space the curve reveals information that does not appear in a trivial manner in the 2D plane. For example, at an $A_1^2 A_1^2$ point of the $\mathcal{SS}$, two curves are intersecting in 2D, but obviously not in 3D, since two different radii were involved. At an $A_1^3$ point, in contrast, three curves still intersect in the 3D space.

On the other hand, points at the $\mathcal{MA}$ or the $\mathcal{SS}$ that arise from locally minimal or maximal circles are clearly visible as local extrema of the 3D curve with respect to the radius.

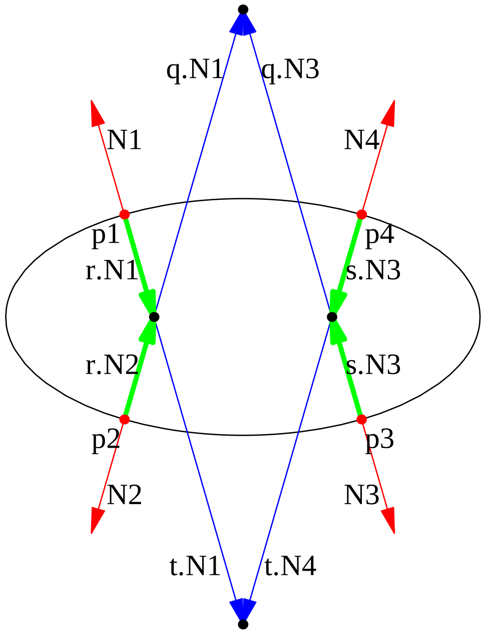


Figure 7: Deriving the Anti Symmetry Set. See text for details.

### 4.3.1 Example

Consider again the ellipse $L(x, y) = x^2 + 4y^2 - 4$. To find the $\mathcal{MA}$ with Eq. 2 we have two points on the shape with $y_1 = -y_2$ and $x_1 = x_2$ and $\tilde{y_1} = \tilde{y_2} = 0$ and $\tilde{x_1} = \tilde{x_2}$ for $(\tilde{x}, \tilde{y})$ a point on the $\mathcal{MA}$. Then $y_1 - 4ry_1/\sqrt{x^2 + 16y_1^2} = y_2 - 4ry_2/\sqrt{x^2 + 16y_2^2}$ yields $r = -\sqrt{x^2 + 16y_2^2}/4$. Together with $y_{1,2} = \pm\sqrt{4 - x^2}$ this gives $r = -\sqrt{16 - 3x^2}/4$. Then the points on the $\mathcal{MA}$ are given by $(\tilde{x}, \tilde{y}, r) = (x + rN, y + rN, r) = (x - x/4, y - 4y/4, -\sqrt{16 - 3x^2}/4) = (3x/4, 0, -\sqrt{16 - 3x^2}/4)$. Note that $x \in [-2, 2]$, so $\tilde{x} \in [-3/2, 3/2]$. The radius varies from $-1/2$ at the endpoints to $-1$ at the origin.

Similarly, one can find the expression for the $\mathcal{SS}$ to be the curve above combined with the curve $(\tilde{x}, \tilde{y}, r) = (0, 3y, -\sqrt{4 + 12y_2^2})$, which varies from $(0, -3, -4)$ via $(0, 0, -2)$ to $(0, 3, -4)$, since $y \in [-1, 1]$. So at the origin in 2D we have an $A_1^2 A_1^2$ point, with radii $2$ and $1$, see Figure 9.

## 4.4 Anti Symmetry Set

Another extension is the Anti-Symmetry Set ($\mathcal{ASS}$). It is defined as the set of points satisfying Eq. (1), but not being part of the symmetry set. Figure 7 clarifies this definition.

The points $p_1$ to $p_4$ have all in common that they give rise to points on the $\mathcal{MA}$ or the $\mathcal{SS}$ in specific pairs. For example, $p_1$ and $p_2$ define a $\mathcal{MA}$ point and $p_1$ and $p_4$ a $\mathcal{SS}$ point. But what about the other combinations with $p_1$? Clearly $p_1$ and $p_3$ satisfy Eq. (1), but they are not on the $\mathcal{SS}$. The same observation can be made for the combination $p_2$ and $p_4$.

These points are part of the so-called anti-symmetry set ($\mathcal{ASS}$): The set of all points satisfying Eq. (1), but not on the $\mathcal{SS}$. The $\mathcal{ASS}$ appeared in the early 1990's due to Blake et al. [6, 5] in the field of robotics. There they considered this set in order to find an optimal finger position for a two finger grasp. Another – perhaps less striking – name is the Mid Parallel Tangent Locus (MPTL), describing exactly what it is, see e.g. [22]:.

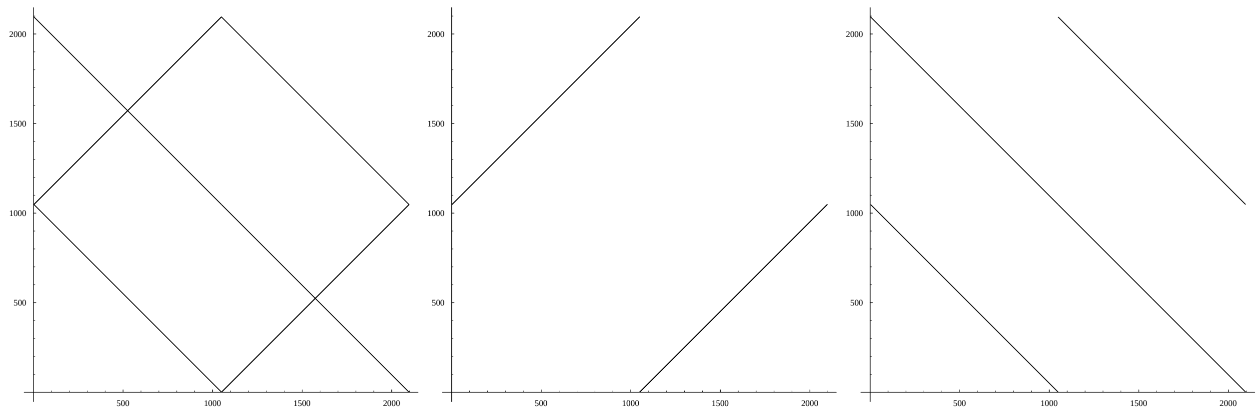


Figure 8: Left to right: The pre-$\mathcal{SS}$, the $\mathcal{ASS}$ part and the $\mathcal{SS}$ part.

## 4.5 Parameter space: Pre Symmetry Set

One way to visualize the locations the signchanges of Eq. (1) is by taking all points on the shape pairwise and plot these signchanges in a diagram. This was used by Holtom [22] and Giblin and Sapiro [17, 19, 4] in a different context (affine symmetry sets). Following their line of reasoning this diagram should be called the pre-$\mathcal{SS}$. This diagram is the representation of the $\mathcal{SS}$ (or the $\mathcal{ASS}$, or the combination of both) in parameter space. Obviously this diagram is symmetric around the diagonal (if the combination $(p_i, p_j)$ has a signchange, then also $(p_j, p_i)$ denotes a signchange). Since the shape is closed, the pre-$\mathcal{SS}$ has cyclic boundaries: if there are $N$ points, the points $p_N$ and $p_1$ are neighbours. So the pre-$\mathcal{SS}$ can be regarded as a union of disjoint simple closed curves on the torus. Some of these intersect the diagonal (representing the evolute in this situation): $(p_i, p_i)$. See also Appendix B.

### 4.5.1 Example

Consider the ellipse – for the last time. The $\mathcal{ASS}$ points are found as those points with $(x_1, y_1) = (-x_2, -y_2)$ and with radii $r = \sqrt{x_1^2 + y_1^2}$), varying between $1$ and $2$. This is identical to the two radii of the $\mathcal{SS}$ at the planar origin, since at these points the $\mathcal{ASS}$ and the $\mathcal{SS}$ intersect. The pre-$\mathcal{SS}$ and the parts of it determining the $\mathcal{SS}$ and the $\mathcal{ASS}$ are shown in Figure 8 from left to right. The diagrams are symmetric in the diagonal $p_i, p_i$. The dark lines represent the zerocrossings of Eq. (1). At intersections of the diagonal and a zerocrossing, a branch of the $\mathcal{SS}$ starts in an $A_3$ point. Since the shape is closed, the lines continue through the boundaries. Therefore the $\mathcal{SS}$ part contains four intersections with the diagonal, corresponding to the four cusps of the evolute. The two lines forming the $\mathcal{SS}$ of the square in the left image consititute one branch of the $\mathcal{SS}$. The long line together with the point at the origin (being a $A_3$ point) forms the second part of the $\mathcal{SS}$. The $\mathcal{ASS}$ image connects the curves. The intersections of the $\mathcal{SS}$ and the $\mathcal{ASS}$ are local extrema w.r.t. radius of the $\mathcal{SS}$, see Figure 9 where the 3D visualization of both sets is shown.

## 4.6 Classification of Points at the (Pre) Symmetry Set

Since numerical localisation in the spatial coordinates is difficult, the parameter space is used to determine the special points (section 2.4). Given the parametrisation, the zerocrossings of Eq. (1) are calculated: these are the locations where $(p_i - p_j).(N_i \pm N_j) = 0$. Secondly, the $\mathcal{ASS}$ points are obtained as the points where $(N_i \pm N_j) = 0$. The intersecting points of both sets points are removed from the former set, yielding the pre-$\mathcal{SS}$. Since curves in the pre- $\mathcal{SS}$ don't intersect, one easily obtains the separate branches. On these branches the points are classified as follows:

- $A_1^2$: All the points of the resulting (symmetry] set are initially classified as $A_1^2$ points.
- $A_3$: At $A_3$ points, one has $p_i = p_j$, since they are located at the diagonal and don't concern two different points on the shape.

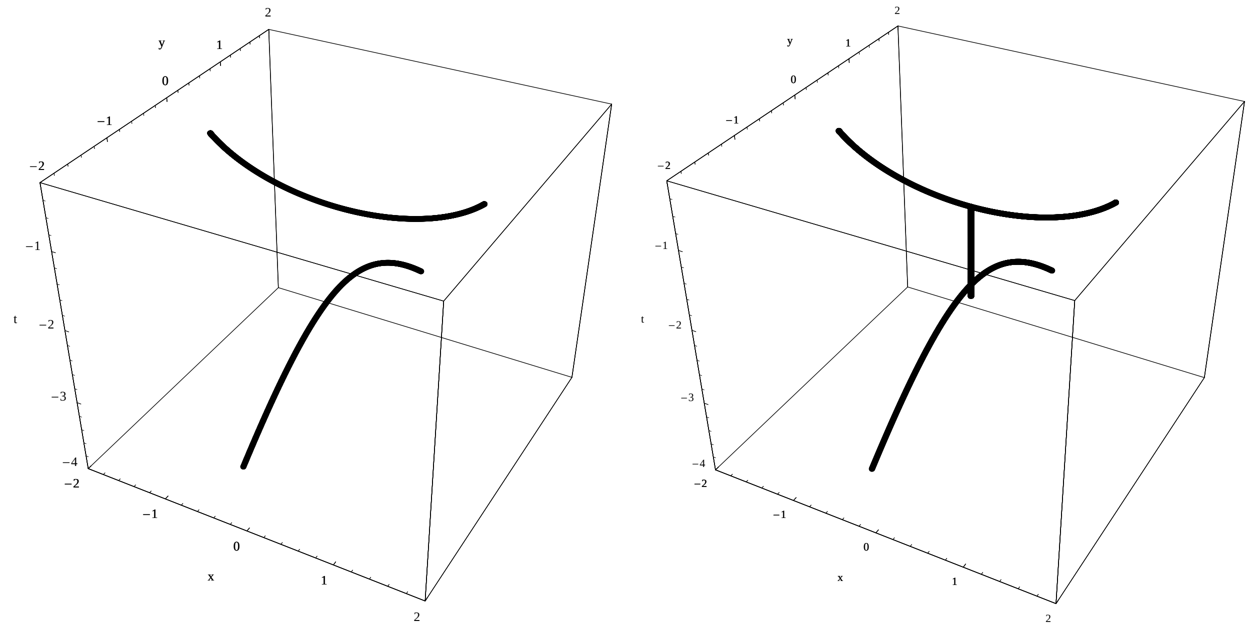


Figure 9: 3D representation of the $\mathcal{SS}$ (left) and the $\mathcal{SS}$ and $\mathcal{ASS}$ (right) of the ellipse.

- $A_1A_2$: **At $A_1A_2$ points the $\mathcal{SS}$ hits the evolute and is reflected. This implies that one of the two involved points, say $p_i$, is also reflected. The pre- $\mathcal{SS}$ therefore has a horizontal or vertical tangent.**
- $A_1^3$: **At an $A_1^3$ point three parts of the $\mathcal{SS}$ intersect. In the pre-$\mathcal{SS}$ these points are detectable as the occurence of the triple pointsets $(p_1, p_2)$, $(p_1, p_3)$, and $(p_2, p_3)$ (and, of course, its diagonal symmetric counterpart).**
- $A_1^2A_1^2$: **At an $A_1^2A_1^2$ point two parts of the $\mathcal{SS}$ intersect. In the pre-$\mathcal{SS}$ these points are not detectable, since they are a result of the projection of the $\mathcal{SS}$ onto the spatial coordinates.**
- **Local extrema w.r.t. radius: These points are the isolated intersections of the $\mathcal{SS}$ and the $\mathcal{ASS}$.**

**Note that the $\mathcal{SS}$ branches can be subdivided into *subbranches*, with endpoints either $A_3$ or $A_1A_2$ points.**

# 5 A Linear Data Structure

**One of the main results with respect to the $\mathcal{SS}$ achieved in [1] is the possibility to represent the $\mathcal{SS}$ as a linear data structure. In general, these structure are faster to query than graph structures - the result of methods based on the $\mathcal{MA}$. The fact that the $\mathcal{SS}$ is a larger, more complicated set than the $\mathcal{MA}$ turns out to be advantageous is generating a simpler datastructure. In this section the structure is described, together with the stability issues. Examples are given in sections 6 and 7.**

## 5.1 Construction of the datastructure

**The datastructure contains the elements described in the previous sections: The $\mathcal{SS}$, its special points and the evolute. They are combined in the following way:**

1. **Take the shape in a parameterized way. This can be achieved for any shape, see Appendix A.**
2. **Get the order of the cusps of the evolute by following the parameterization.**
3. **Line the cusps up.**

4. Find for the $\mathcal{SS}$ the $A_3$ points: they form the end of individual branches.
5. Relate each cusp of the evolute go an $A_3$ point.
6. Link the cusps that are on the same branch of the $\mathcal{SS}$.
7. Augment the links with labels, related to the other special points that take place when traveling from one cusp point to the other along the $\mathcal{SS}$-branch.
8. Assign the same label to different branches if an events involves the different branches: the crossings at $A_1^3$ (three identical labels) and $A_1^2/A_1^2$ (two identical labels) points. The latter can be left out, since they occur due to projection.
9. Insert moth branches (explained below) between two times two cusps as void cusps.
10. Done.

Moth branches are $\mathcal{SS}$ branches without $A_3$ points. They contain four $A_1A_2$ points, that are located on the evolute. Each point is connected by the $\mathcal{SS}$ branch to two other points along the moth. In the pre-$\mathcal{SS}$ they appear as closed loops that do not intersect the diagonal.

The datastructure thus contains the $A_3$ points in order, links between pairs of them and augments along the links. Alternatively, one can think of a construction of a set of strings (the links), where each string contains the special points of the $\mathcal{SS}$ along the branch represented by the string.

## 5.2 Modified datastructure

Since the introduction of void cusps due to moth branches violates the idea of using only the $A_3$ points as nodes, a modified structure can be used as well. In this structure the nodes contain $A_3$ and $A_1A_2$ points. These can be lined up easily, since the $A_1A_2$ points are located on the evolute between $A_3$ points. The linked connections made (strings) are now the subbranches of the $\mathcal{SS}$. The augmentation now only consists of the crossings of subbranches (either at $A_1^3$, or at both $A_1^3$ and $A_1^2/A_1^2$).

## 5.3 Transitions

In this section the known transitions of the $\mathcal{SS}$ [10] in relation to the proposed datastructure [18] is presented.

### 5.3.1 $A_1^4$

At an $A_1^4$ transition a collision of $A_1^3$ points appears. Before and after the transition six lines, four $A_1^3$ points and three $A_1^2/A_1^2$ occur. The result on the $\mathcal{MA}$ is a reordering of the connection of two connected Y-parts of the skeleton. For the $\mathcal{SS}$, however, the Y-parts are the visible parts of $\mathcal{SS}$ branches going through $A_1^3$ points. So for the $\mathcal{SS}$ representation nothing changes.

### 5.3.2 $A_1A_3$

At an $A_1A_3$ transition, a cusp of the evolute (and thus an endpart of a $\mathcal{SS}$ branch including a $A_3$ point) intersects a branch of the $\mathcal{SS}$ and an $A_1^3$ point as well as two $A_1A_2$ points are created or annihilated. The $A_1^3$ point lies on the $A_3$ containing branch, while the other branch contains a "triangle´´ with the $A_1^3$ and the $A_1A_2$'s as cornerpoints: the strings $A_3[1] - a$ and $b$ change to $A_3[1] - A_1^2/A_1^2[1] - A_1^3[1] - a$ and $b_1 - A_1^3[1] - A_1A_2[1] - A_1^2/A_1^2[1] - A_1A_2[2] - A_1^3[1] - b_2$, vice versa.

### 5.3.3 $A_4$

The $A_4$ transition corresponds to creation or annihilation of a swallowtail structure of the evolute and the creation or annihilation of the enclosed $\mathcal{SS}$ branch with two $A_3$ and two $A_1A_2$ points: the string $A_3[1] - A_1^2/A_1^2[1] - A_1A_2[1] - A_1A_2[2] - A_1^2/A_1^2[1] - A_3[2]$.

### 5.3.4 $A_1^2A_2$

**At an $A_1^2A_2$ transition two non-intersecting $A_1A_2$-containing branches meet a third $\mathcal{SS}$ branch at the evolute, creating two times three different branches intersecting at two $A_1^3$ points. Or the inverse transition occurs: the strings $a$, $b_1 - A_1A_2[1] - b_2$ and $c_1 - A_1A_2[2] - c_2$ become $a_1 - A_1^3[1] - A_1^3[2] - a_3$, $b_1 - A_1^3[1] - A_1A_2[1] - A_1^2/A_1^2[1] - A_1^3[2] - b_2$ and $c_1 - A_1^3[1] - A_1^2/A_1^2[1] - A_1A_2[2] - A_1^3[2] - c_2$, vice versa.**

### 5.3.5 $A_2^2$ moth

**The $A_2^2$ moth transition describes the creation or annihilation of a $\mathcal{SS}$ branch containing only four $A_1A_2$ and no $A_3$ points. These points lie pairwise on two opposite parts of the evolute. each point is connected via the $\mathcal{SS}$ to the two points on the opposite part of the evolute: the strings $A_1A_2[1] - A_1^2/A_1^2[1] - A_1A_2[3] - A_1A_2[2] - A_1^2/A_1^2[1] - A_1A_2[4]$, if the pairs 1,2 and 3,4 are one the same part of the evolute.**

### 5.3.6 $A_2^2$ nib

**When going through an $A_2^2$ nib transition, two branches of the $\mathcal{SS}$, each containing an $A_1A_2$ point, meet and exchange a subbranch. The strings $a - A_1A_2[1] - b$ and $c - A_1A_2[2] - d$ become $a - A_1A_2[1] - c_1 - A_1^2/A_1^2[1] - c_2$ and $b_1 - A_1^2/A_1^2[1] - b_2 - A_1A_2[2] - d$.**

### 5.3.7 Stability

**The possible transitions as given above invoke only deletion, insertion or reordering of special points or branches on the datastructure in an exact and pre-described manner. It is therefore a robust and stable description of the original shape.**

# 6 Example I: the Cubic Oval

**As first example the closed part of a cubic oval is taken, which is implicitly given by $f(x, y; a, b) = 2bxy + a^2(x - x^3) - y^2 = 0$ and $x \geq 0$. Figure 10 shows this shape for $a = 1.025$ and $b = 0.09, 0.15, 0.30$. Changing one of these parameters, one is likely to encounter one of the transitions described above. On this shape with these values for the parameters, six extrema of the curvature occur, while the curvature doesn't change sign and the shape is thus convex. Firstly the case $a = 1.025$ and $b = 0.09$ is considered [8].**

## 6.1 Symmetry Set and Anti-Symmetry Set, 2D

**The two extra extrema of the curvature, compared to the ellipse, arise from a perturbation of the shape involving an $A_4$ transition[1]. A direct consequence is that a new branch of the $\mathcal{SS}$ is created. In Figure 11a the complete $\mathcal{SS}$ with the evolute and a part of the shape as visualized. The newly created branch has the shape of a swallowtail, as expected from the $A_4$ transition. Figure 11b, shows that three curves joining pairwise in cusps for the ASS.**

## 6.2 Symmetry Set and Anti-Symmetry Set, 3D

**More details can be seen in the 3D representation, Figure 12.**

**Since the extrema of the curvature alternate along the shape, a maximum and a minimum are created. As a prerequisite of the $A_4$ transition, the evolute is self-intersecting. Furthermore, the evolute contains six cusps. A direct consequence is that the new branch of the $\mathcal{SS}$ that is created, since branches always start in the cusps, must be essentially different from the two other branches, since the original branches start in cusps that both arise from either local maxima of the curvature, or minima. These $\mathcal{SS}$ curves essentially need to have a local extremum with respect to the radius in 3D. The newly created branch, however, has a endpoints due to a minimum and a maximum of the curvature, so its behaviour in 3D must be different. This is shown in Figure 12a, where the two "old" branches are parabola-shaped, with an extremum. The swallowtail has maxima at**

[1]For $b = 0$ and $a = .5$ an egg-shape is obtained with a $\mathcal{SS}$ similar to the ellipse, although the vertical branch is curved.

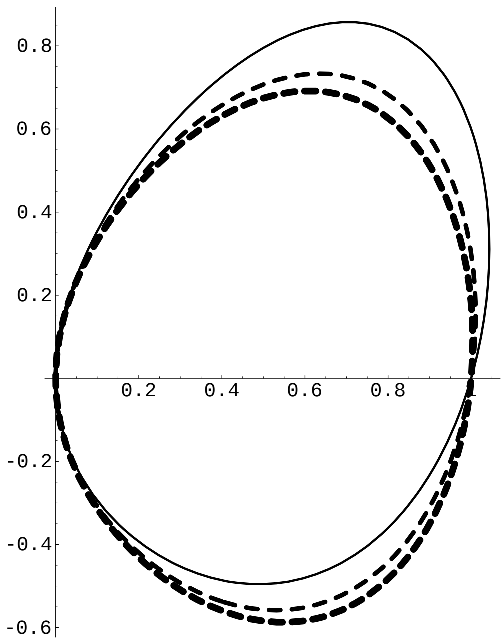


Figure 10: The cubic oval for $b = .09$ (thick, dashed), $b = .15$ (intermediate thickness, dashed), and $b = .15$ (thin, continuous).

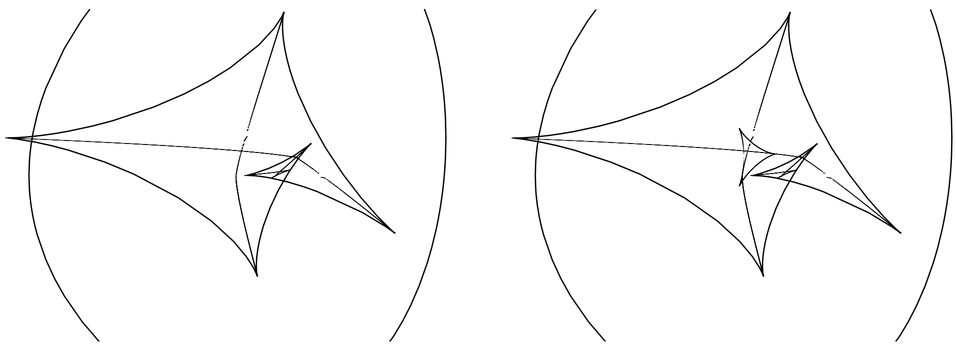

Figure 11: 2D representation of the $\mathcal{SS}$ (left) and the $\mathcal{SS}$ with the $\mathcal{ASS}$ (right) of the cubic oval.

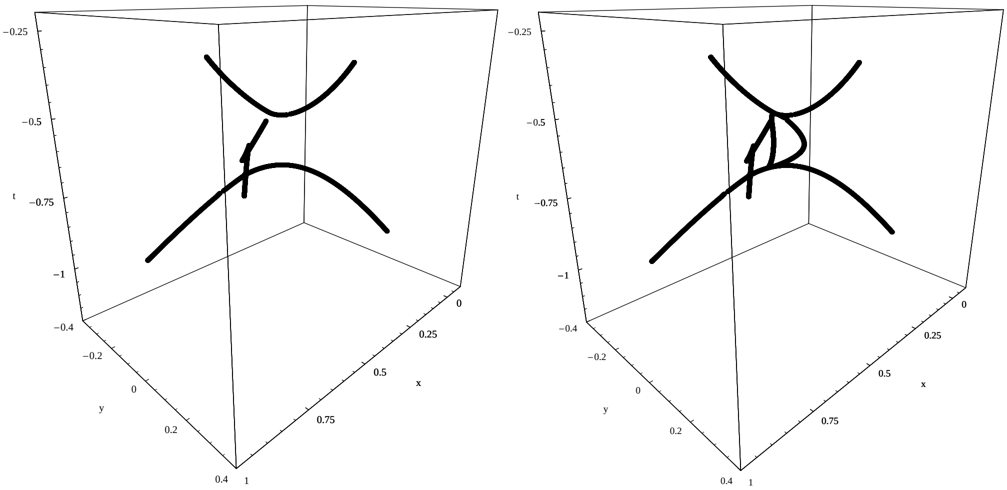


Figure 12: 3D representation of the $\mathcal{SS}$ (left) and the $\mathcal{SS}$ with the $\mathcal{ASS}$ (right) of the cubic oval.

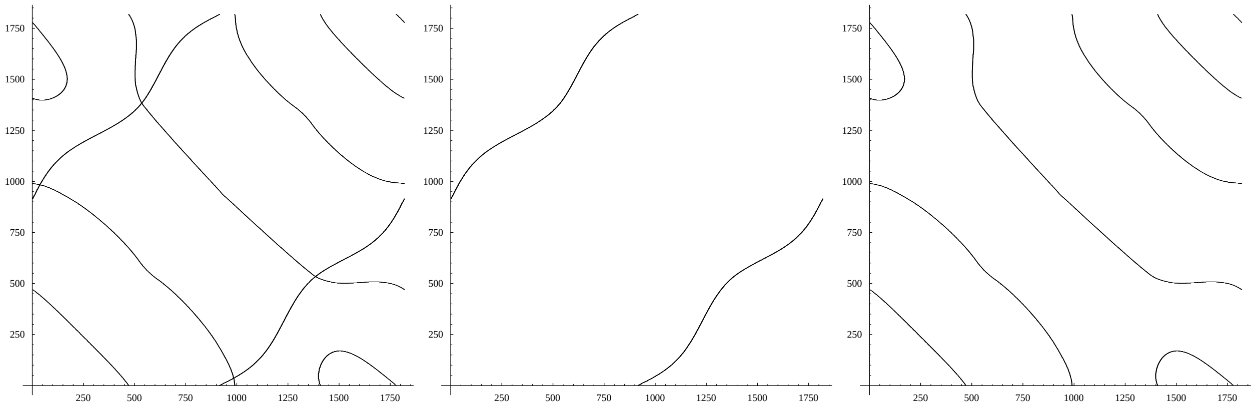


Figure 13: Left to right: The pre-$\mathcal{SS}$, the $\mathcal{ASS}$ part and the $\mathcal{SS}$ part of the cubic oval.

one pair of $A_3$ and $A_1A_2$ points, and minima on the pair. It also intersects the lower parabola. Since real intersections - $A_1^3$ points - always involve 3 segments, a close-up is needed there.

The 3D $\mathcal{ASS}$ part, Figure 12b, shows that although the 2D projection may look like a combination of 3 cusps, it is in fact a closed loop. The ellipse had one straight vertical line, but a perturbation shows that this was in fact a combination of two lines: one due to the pointset $(x, y), (-x, -y)$, and one due to $(x, -y), (-x, y)$. For the oval they become visible as two separate curves joining extrema of the parabolas.

## 6.3 Pre-Symmetry Set

The behaviour of the pre-$\mathcal{SS}$ is also different: a new branch implies a new curve in the pre-$\mathcal{SS}$. Since the perturbation is a local effect, not all points on the shape are involved in creation the new branch. The curve in the pre-$\mathcal{SS}$ thus must be a closed loop. This is indeed what occurs in Figure 13, where the loop continue a along the boundaries. Counting the $A_3$ points along the diagonal, the loop contains the points at position 5 and 6 (subsequent, because two subsequent extrema of the curvature were created). The other curves contain $A_3$'s at position 1 and 3, and 2 and 4 (odd and even, since each pair corresponds to the same kind of extrema).

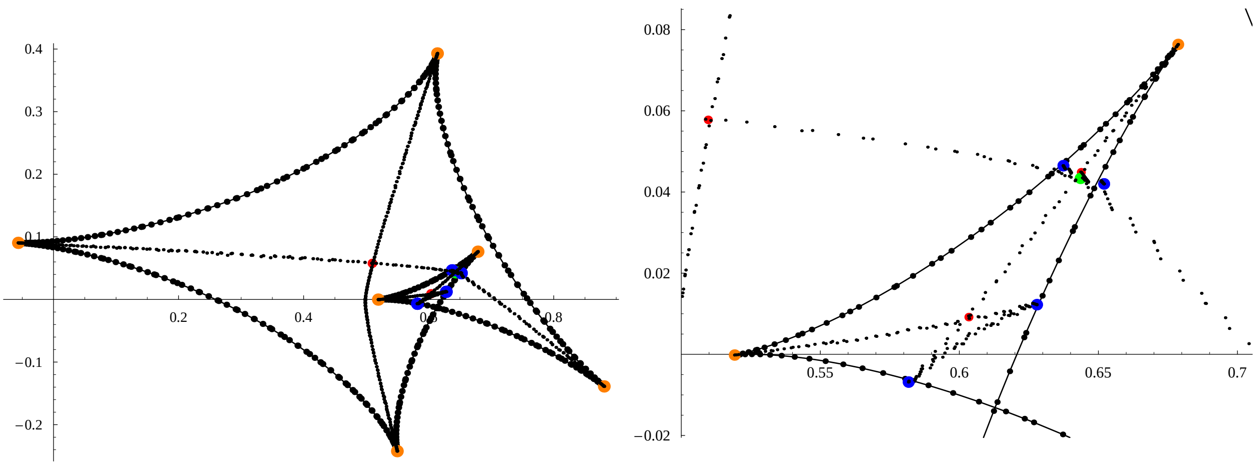


Figure 14: 2D representation of the $\mathcal{SS}$ (left) and a close-up (right) of the oval, $b = 0.09$. The contour with points is the evolute.

## 6.4 Symmetry Set, 2D augmented

**The newly created branch introduces besides the $A_3$ and $A_1^2/A_1^2$ points the other types of special points, viz. the $A_1^3$ and $A_1A_2$ points, as shown in Figure 14a. The points are marked with dots on top of them. There are six $A_3$ points on the cusps of the evolute, four $A_1A_2$ points on the evolute close to the selfintersection part, three $A_1^2/A_1^2$ points and one $A_1^3$ point. The latter can be seen in more detail in the close-up in Figure 14b. It is close to two $A_1A_2$ points and an $A_1^2/A_1^2$ point**

## 6.5 Data Structure

**To obtain the datastructure, the first cusp of the evolute ($A_3$ of the $\mathcal{SS}$), is the one in the middle at the bottom. The others are taken clockwise. Then the $\mathcal{SS}$ consists of the branches $1-3$, $2-4$, and $5-6$. Branch $1-3$ intersects $2-4$ at the first $A_1^2/A_1^2$ point. The close-up of the branch $4-5$, Figure 14b, gives insight in the behaviour around this part of the $\mathcal{SS}$.**

**Both the branches $2-4$ and $5-6$ each contain two $A_1A_2$ points. Both branches intersect at an $A_1^3$ point, which is close to the two $A_1A_2$ points of branch $2-4$: At this point two subbranches of branch $2-4$ (the ones combing the $A_3$'s with the $A_1A_2$'s) and branch $4-5$ intersect. Just above this point, branch $5-6$ intersects a subbranches of branch $2-4$ (the one combing the $A_1A_2$'s) in the second $A_1^2/A_1^2$ point. Finally, two subbranches of branch $2-4$ (the ones combing the $A_3$'s with the $A_1A_2$'s) intersect at the third $A_1^2/A_1^2$ point.**

**So the datastructure is given by the string $A_3[1]-A_3[2]-A_3[3]-A_3[4]-A_3[5]-A_3[6]$ and the links (see also Figure 15, top):**

1. $A_3[1]-A_1^2/A_1^2[1]-A_3[3]$
2. $A_3[2]-A_1^2/A_1^2[1]-A_1^3[1]-A_1A_2[1]-A_1^2/A_1^2[2]-A_1A_2[2]-A_1^3[1]-A_3[4]$
3. $A_3[5]-A_1^2/A_1^2[3]-A_1A_2[3]-A_1A_2[4]-A_1^2/A_1^2[3]-A_1^3[1]-A_1^2/A_1^2[2]-A_3[6]$

**The modified datastructure is given by the string $A_3[1]-A_3[2]-A_3[3]-A_3[4]-A_1A_2[4]-A_3[5]-A_1A_2[2]-A_3[6]-A_1A_2[1]-A_1A_2[3]$ and the links (see Figure 15, bottom):**

1. $A_3[1]-A_1^2/A_1^2[1]-A_3[3]$
2. $A_3[2]-A_1^2/A_1^2[1]-A_1^3[1]-A_1A_2[1]-$
3. $A_1A_2[1]-A_1^2/A_1^2[2]-A_1A_2[2]$
4. $A_1A_2[2]-A_1^3[1]-A_3[4]$

5. $A_3[5] - A_1^2/A_1^2[3] - A_1A_2[3]$
6. $A_1A_2[3] - A_1A_2[4]$
7. $A_1A_2[4] - A_1^2/A_1^2[3] - A_1^3[1] - A_1^2/A_1^2[2] - A_3[6]$

This representation clearly decreases the number of augments, but increases the number of points along the string, and thus the number of links. The difference along the sting between $A_3$ points and $A_1A_2$ points is due to the number of links starting and ending at a point. An $A_3$ point has one link, an $A_1A_2$ point two. Note that ignoring the projective $A_1^2/A_1^2$ points, the second datastructure contains only $A_1^3$ points as augments.

## 6.6 Transitions

When $b$ is increased the shape modifies according to Figure 10. The symmetry set changes also when $b$ is increased. At two stages a "significant" change takes place: one of the aforementioned transitions. In the following sections the resulting symmetry sets and datastructures after the transitions are given. Note that it is non-generic to encounter a situation at which a transition occurs.

### 6.6.1 Annihilation of the $A_1^3$ point

When $b$ increases to $0.15$, branch $4-5$ releases branch $2-6$, see Figure 16, annihilating the involved special points. This is a typical example of an $A_1A_3$ transition.

De first datastructure is now given by the string $A_3[1] - A_3[2] - A_3[3] - A_3[4] - A_3[5] - A_3[6]$ and the links (see also Figure 17, top):

1. $A_3[1] - A_1^2/A_1^2[1] - A_3[3]$
2. $A_3[2] - A_1^2/A_1^2[1] - A_3[4]$
3. $A_3[5] - A_1^2/A_1^2[3] - A_1A_2[3] - A_1A_2[4] - A_1^2/A_1^2[3] - A_3[6]$

The modified datastructure is given by the string $A_3[1] - A_3[2] - A_3[3] - A_3[4] - A_1A_2[4] - A_3[5] - A_3[6] - A_1A_2[3]$ and the links (see also Figure 17, bottom):

1. $A_3[1] - A_1^2/A_1^2[1] - A_3[3]$
2. $A_3[2] - A_1^2/A_1^2[1] - A_3[4]$
3. $A_3[5] - A_1^2/A_1^2[3] - A_1A_2[3]$
4. $A_1A_2[3] - A_1A_2[4]$
5. $A_1A_2[4] - A_1^2/A_1^2[3] - A_3[6]$

### 6.6.2 Creation of an $A_1^3$ point

When $b$ increases further to $b = 0.30$, again an $A_1A_3$ transition occurs, this time the other way round. Now branch $4-5$ intersects branch $1-3$, creating the necessary involved special points, see Figure 18.

De first datastructure is now given by the string $A_3[1] - A_3[2] - A_3[3] - A_3[4] - A_3[5] - A_3[6]$ and the links (see also Figure 19, top):

1. $A_3[1] - A_1^3[1] - A_1A_2[1] - A_1^2/A_1^2[2] - A_1A_2[2] - A_1^3[1] - A_1^2/A_1^2[1] - A_3[3]$
2. $A_3[2] - A_1^2/A_1^2[1] - A_3[4]$
3. $A_3[5] - A_1^2/A_1^2[2] - A_1^3[1] - A_1^2/A_1^2[3] - A_1A_2[3] - A_1A_2[4] - A_1^2/A_1^2[3] - A_3[6]$

The modified datastructure is given by the sequence $A_3[1] - A_3[2] - A_3[3] - A_3[4] - A_1A_2[4] - A_1A_2[2] - A_3[5] - A_1A_2[1] - A_3[6] - A_1A_2[3]$ and the links (see also Figure 19, bottom):

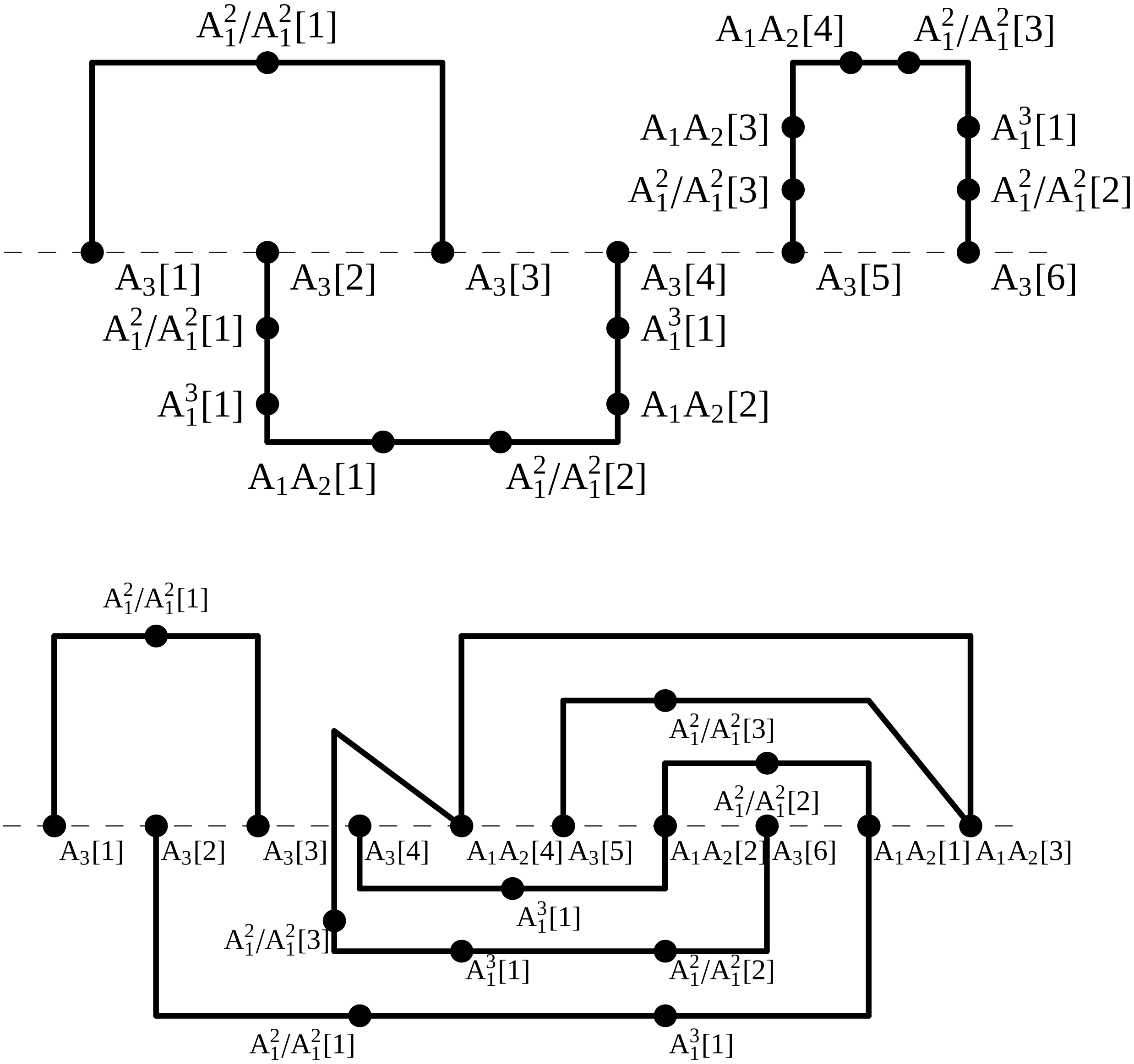


Figure 15: String representations of the $\mathcal{SS}$ of the oval, $b = 0.09$.

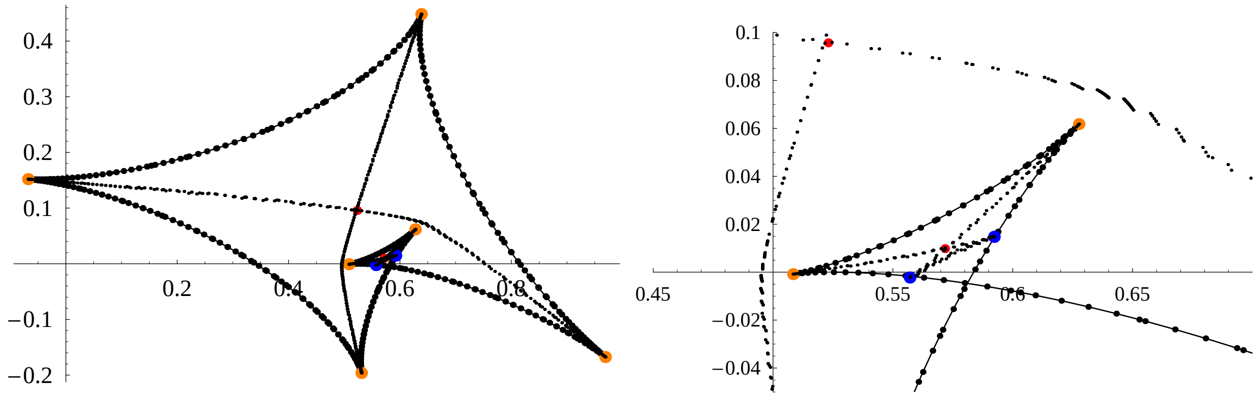


Figure 16: 2D representation of the $\mathcal{SS}$ (left) and a close-up (right) of the oval, $b = 0.15$. The contour with points is the evolute.

1. $A_3[1] - A_1^3[1] - A_1A_2[1]$
2. $A_1A_2[1] - A_1^2/A_1^2[2] - A_1A_2[2]$
3. $A_1A_2[2] - A_1^3[1] - A_1^2/A_1^2[1] - A_3[3]$
4. $A_3[2] - A_1^2/A_1^2[1] - A_3[4]$
5. $A_3[5] - A_1^2/A_1^2[2] - A_1^3[1] - A_1^2/A_1^2[3] - A_1A_2[3]$
6. $A_1A_2[3] - A_1A_2[4]$
7. $A_1A_2[4] - A_1^2/A_1^2[3] - A_3[6]$

One can verify that the structure obtained for $b = 0.09$ and $b = 0.30$ are not identical up to rotational invariance due to the ordering of the cusps of the evolute. With respect to the $\mathcal{MA}$ representation, the first $A_1^3$ point does not contribute to the $\mathcal{MA}$, since the $\mathcal{MA}$ consists of the connected component in the 3D representation with the smallest radius, i.e. the most upper connected part. For $b = 0.09$, this is only a curve (the vertical oriented one of the $\mathcal{SS}$). For $b = 0.30$, however, the swallowtail intersects this part and the $\mathcal{MA}$-skeleton now contains an extra branch, pointing from the $A_1^3$ point to the left. This event is known as an instability of the $\mathcal{MA}$.

# 7 Example II: A Concave Shape

The previous section dealt with a convex shape. This simplifies the structure of the evolute, since it also is a closed shape. For concave shapes, the curvature $\kappa$ becomes zero at some points, and the evolute is not defined at those points. Recall that the evolute is given by $\mathcal{S} + \mathcal{N}/\kappa$. If the points at infinity are added, again a closed shape is obtained. As an example the function $f(x, y; a, b) = (x^2 - xy/5 + y^2 + a^2)^2 - b^2 - 4a^2x^2$ is taken and the shape for $f = 0$ with $a = 1.99$ and $b = 4$ is shown in Figure 21a. Figure 21b shows the evolute connecting the four cusps. The image includes the four asymptotes to which the evolute converges at (minus) infinity. One can see that the evolute starting in a cusp, moves towards infinity and continues at the other side of the straight line representing the asymptotes at minus infinity, towards the next cusp, and so on.

The pre-$\mathcal{SS}$, shown in Figure 22, does not show any 'infinity' behaviour - since it appears in the parameter space -, although the $\mathcal{ASS}$ part shows some extra closed loops. The $\mathcal{SS}$ part, however, is very simple and even similar to that of an ellipse: Two branches and four $A_3$ points. There are no $A_1A_2$ points (and thus no $A_1^3$ points).

Consequently, the $\mathcal{SS}$ of this shape is expected to consist of two branches connecting the two pairs of $A_3$ points, crossing at an $A_1^2/A_1^2$ point. Due to the shape of the evolute, this can only be achieved if the branch of

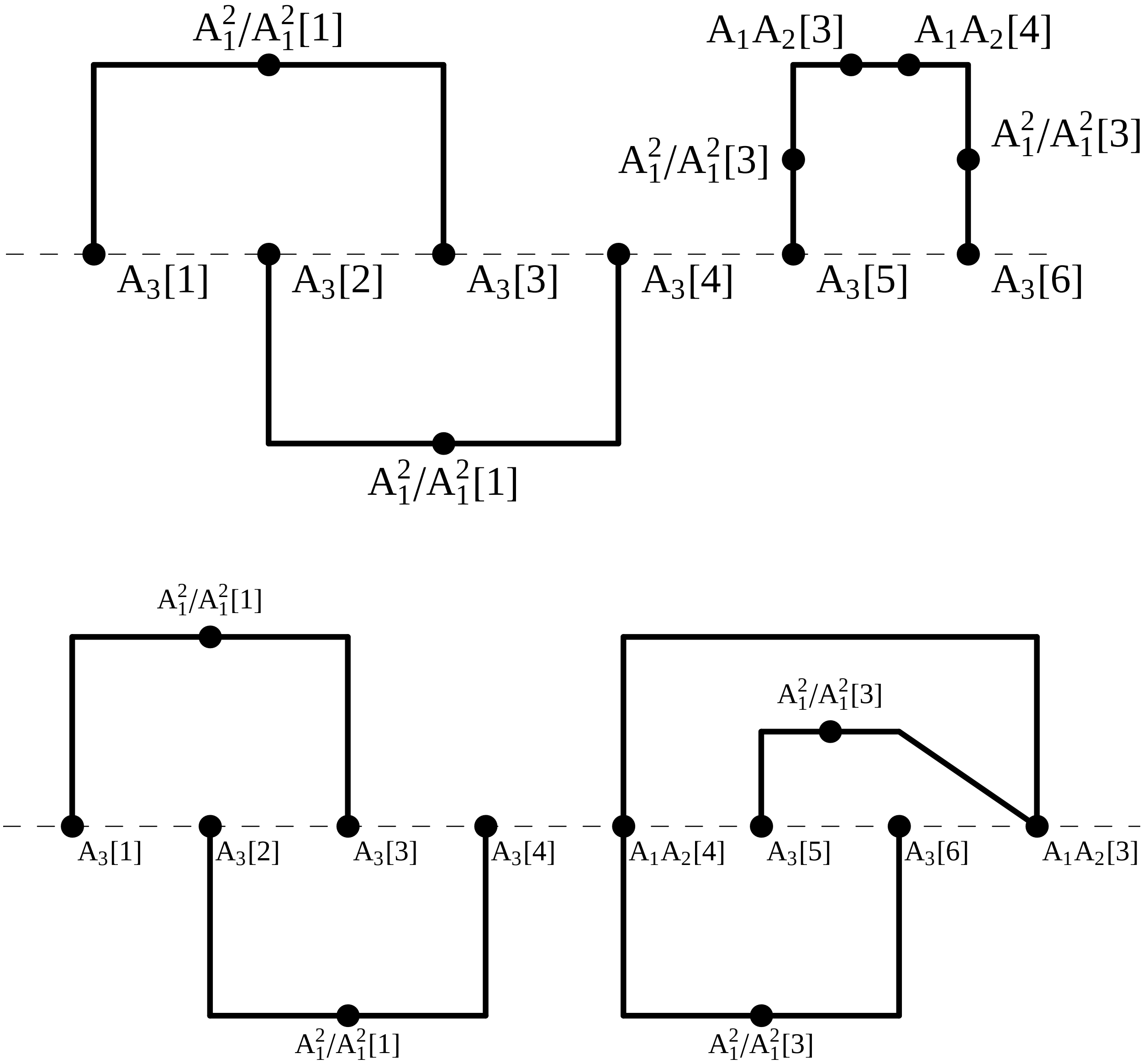


Figure 17: String representations of the $\mathcal{SS}$ of the oval, $b = 0.15$.

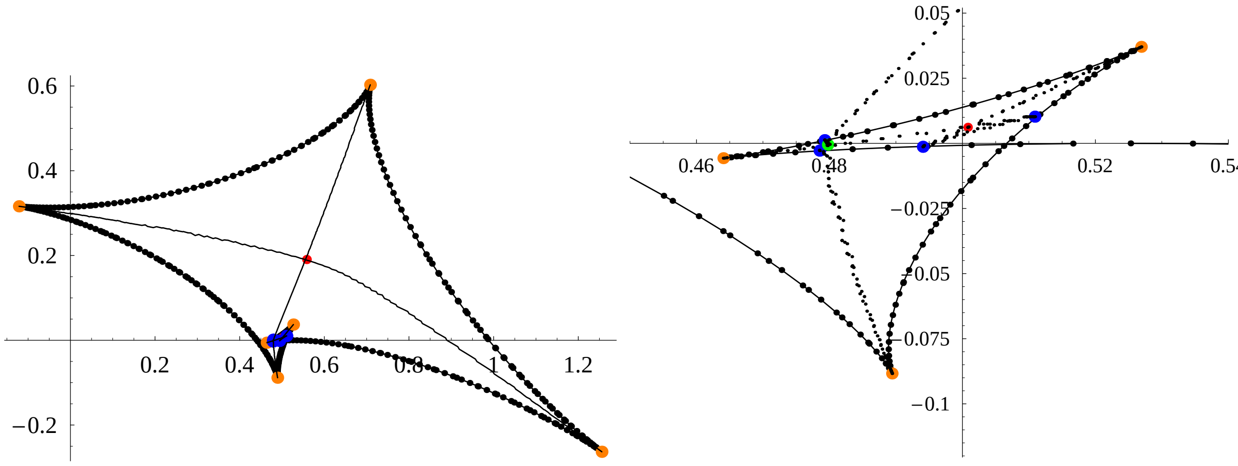


Figure 18: 2D representation of the $\mathcal{SS}$ (left) and a close-up (right) of the oval, $b = 0.30$. The contour with points is the evolute.

**the $\mathcal{SS}$ connecting the $A_3$ points lying almost at the $y$-axis, passes infinity twice. This is exactly what can be seen in Figure 23.**

**To see what happens along this branch of the $\mathcal{SS}$, see Figure 24a. This image shows four circles defining points on the $\mathcal{SS}$. The first is the one on the $A_3$ point, resulting in the smallest circle, due to the minimal curvature of the shape at the 'neck' between the two bubbles. The next circle touches at two points close to this neck, resulting in a point at some distance of the $A_3$ point on the $\mathcal{SS}$.**

**This continues for the next two circles until the point on the $\mathcal{SS}$ reaches infinity. There the circle is tangent at the two points on the shape, that have identical normals and are connected by a line tangent at these points. In Figure 24b these points are dotted. On the other hand, at these two points, also the circle on the $\mathcal{SS}$ branch at minus infinity touches the shape. So these points give rise to a special $A_1^2/A_1^2$ point, viz. one with the radii $\pm\infty$. Continuing along the $\mathcal{SS}$, the branch passes the origin, where a normal $A_1^2/A_1^2$ point occurs, with radii representing the minimal distance connecting the top and bottom at the neck, and the maximal distance connecting the left and right sides of the shape. Next, the $\mathcal{SS}$ heads towards infinity and thus a special $A_1^2/A_1^2$ is again encountered, when two circles are tangent to the shape at the two points dotted at the lower part of it. Figure 24b shows the four points where the circles with radii $\pm\infty$ at the special $A_1^2/A_1^2$ are tangent to the shape, as well as four parts of circles close to these two circles.**

**The special $A_1^2/A_1^2$ can be found easily in the 3D representation with spatial coordinates and the radius: there the $\mathcal{SS}$ simply changes radius from largely positive to largely negative, or vice versa.**

**In the pre-$\mathcal{SS}$ they are part of the points being also present at the $\mathcal{ASS}$, since the normals are identical. In Figure 22a and b four closed loops can be seen. The two on the diagonal are due to zero's of $N_1 - N_2$, the other two and the two line segments in Figure 22b are due to zero's of $N_1 + N_2$. Since the points of currently interest do not cancel out eachother due to opposite signs, but to the fact that they are parallel, they are the part of the intersection of the two "$N_1 - N_2 = 0$"-loops of the $\mathcal{ASS}$, Figure 22b, with the $\mathcal{SS}$, Figure 22c.**

## 7.1 Data Structure

**The according datastructure is thus derived as**

- $A_3[1] - A_1^2/A_1^2[\infty_1] - A_1^2/A_1^2[1] - A_1^2/A_1^2[\infty_2] - A_3[3]$
- $A_3[2] - A_1^2/A_1^2[1] - A_3[4]$

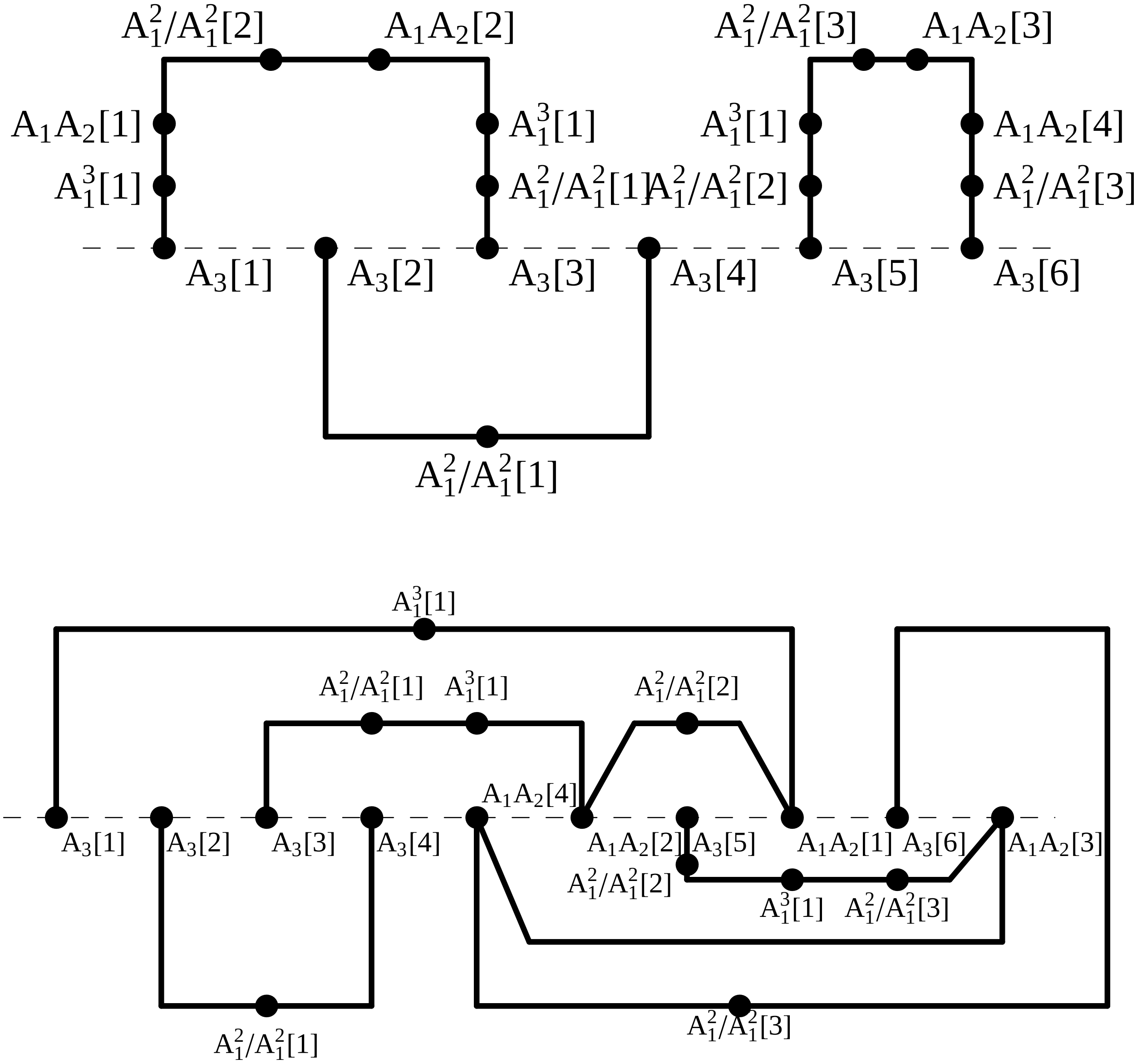


Figure 19: String representations of the $\mathcal{SS}$ of the oval, $b = 0.15$.

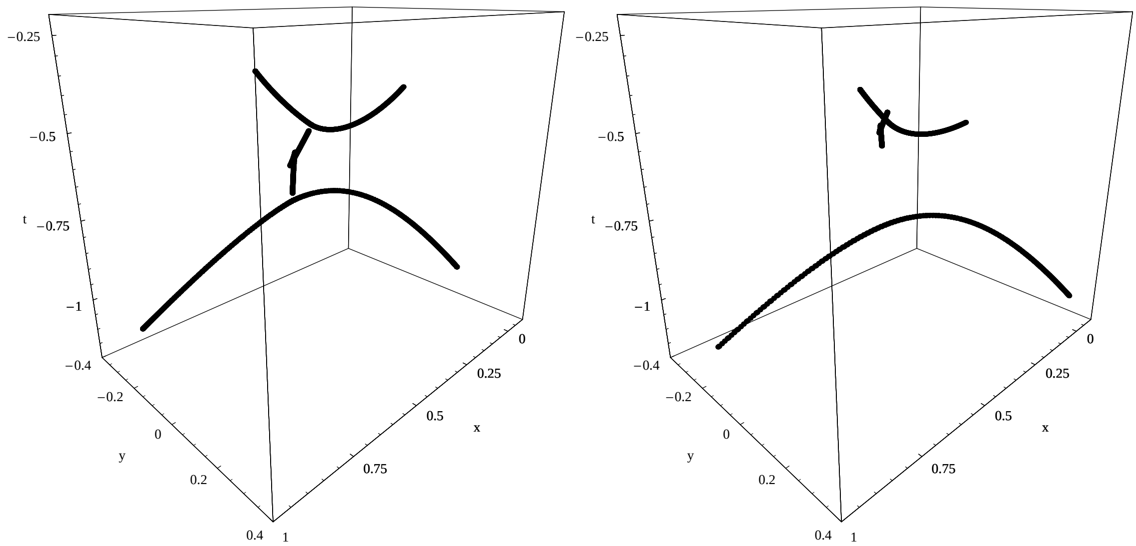


Figure 20: 3D representation of the $\mathcal{SS}$ of the cubic oval for $b = .15$ (left) and $b = .30$ (right) .

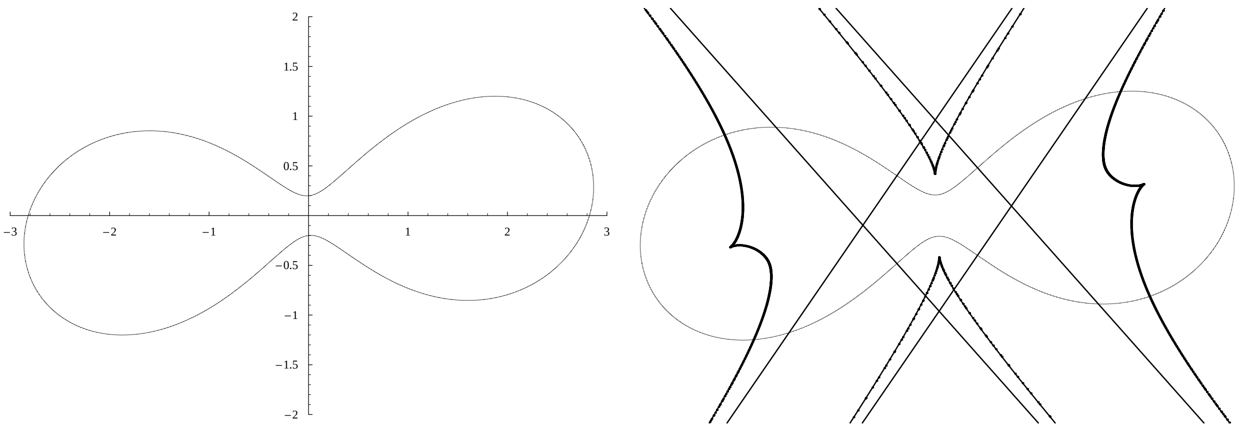


Figure 21: Concave shape (left) and the shape with its evolute, including the asymptotes for $\kappa = 0$, the straight lines. (right).

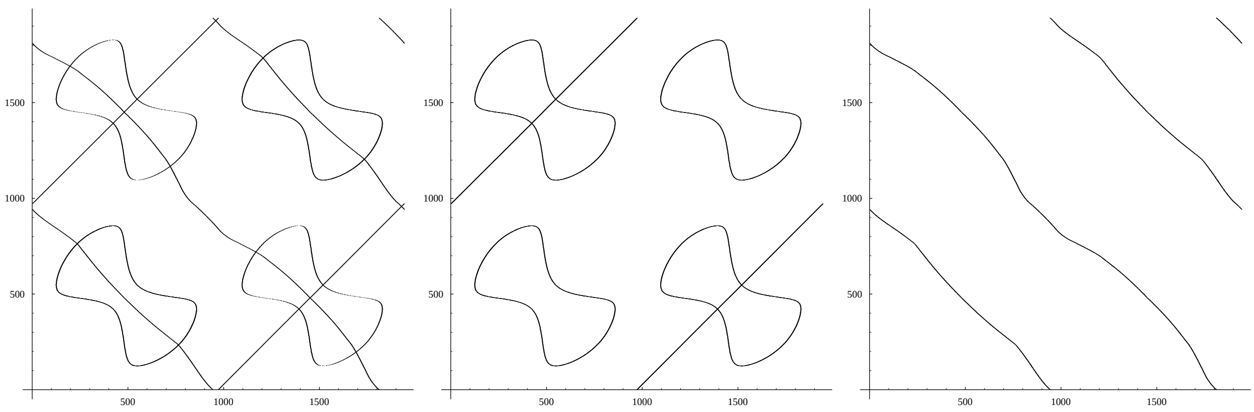


Figure 22: Left to right: The pre-$\mathcal{SS}$, the $\mathcal{ASS}$ part and the $\mathcal{SS}$ part of the concave shape.

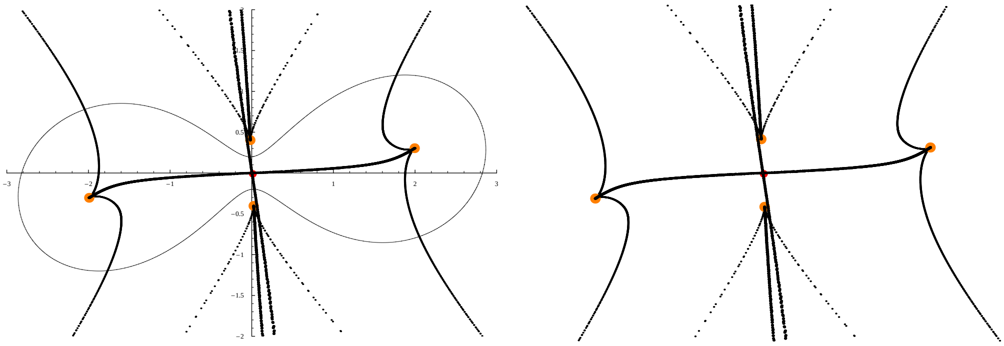

Figure 23: The concave shape and its $\mathcal{SS}$ (left), only the $\mathcal{SS}$ (right).

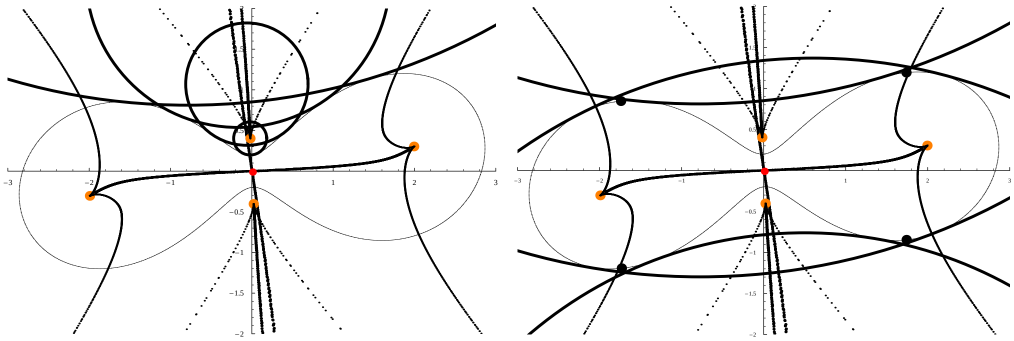

Figure 24: Left: The concave shape, its $\mathcal{SS}$ and four (parts of) tangent circles with radii increasing to infinity. Right: Two pairs of circles with almost infinite radius, located at either plus infinity or minus infinity. At the two pairs of points the circle at plus and minus infinity coincide- i.e. the circle has become a straight line.

# 8 Conclusions

**In this paper a new linear datastructure representing the symmetry set ($\mathcal{SS}$) is presented. This structure depends on the ordering of the cusps of the evolute - related to the local extrema of the curvature of the shape, as well as the $A_3$ points on the $\mathcal{SS}$. The $A_3$ points are also the endpoints of the branches of the $\mathcal{SS}$. Cusps of the evolute that are connected by the $\mathcal{SS}$ are linked in this datastructure. Special points on the $\mathcal{SS}$ (where it touches the evolute, the $A_1A_2$ points, as well as intersection points - both real and those due to projection) are augmented on these links. A modified datastructure takes all the points with evolute interaction - the $A_3$ and the $A_1A_2$ points - into account, again in order along the evolute.**

**Although the $\mathcal{SS}$ is a larger set than the Medial Axis ($\mathcal{MA}$) - even containing it - the representing string structure is in complexity simpler than that for the $\mathcal{MA}$, which yields a graph structure. This allows fast algorithms for the comparison of different shapes, as well as (large) database queries. The richer complexity of the $\mathcal{SS}$ prevents it from instabilities that occur in the $\mathcal{MA}$. These instabilities are due to parts of the $\mathcal{SS}$ that "suddenly" ,i.e. due to certain well-known transitions, become visible.**

**Secondly, two previously unexplored ways of representing the $\mathcal{SS}$ itself are presented and used. The first representation extends the common 2D visualization to 3D by including the distance from the $\mathcal{SS}$ to the shape as an extra dimension. The second representation, called pre-$\mathcal{SS}$, is done parameter space. Both representations reveal the richness of the $\mathcal{SS}$ in more detail than the common 2D visualization and can be used to derive the aforementioned datastructure efficiently.**

**Thirdly, an investigation of possible methods to calculate the $\mathcal{SS}$ has been carried out. Since the $\mathcal{MA}$ can be found by fast implementations of partial differential equations (PDEs), the focus was on PDE methods to calculate the $\mathcal{SS}$. However, due to the definition and thus properties of the $\mathcal{SS}$, PDEs (and modifications of them) are impossible to use. The only way to derive the $\mathcal{SS}$ is therefore by means of a direct implementation of its geometric definition. The complexity of the obtained algorithm is quadratic in the number of points on the shape.**

**Examples of the datastructures and the visualization methods are given on a convex and a concave shape. Stability issues are discussed in relation to the known transitions, the significant changes of the $\mathcal{SS}$. Their description is translated in terms of the datastructures, showing its stability and robustness.**

**A *Mathematica* notebook (program) has been written to derive the datastructures, the visualizations of the $\mathcal{SS}$ in 2D and 3D, transitions of them, and the pre-$\mathcal{SS}$ Details can be found in Appendix A.**

**Still some theoretical questions with respect to the datastructure, the $\mathcal{SS}$ and the pre-$\mathcal{SS}$ are open, of which some are mentioned in Appendix B. Although these questions are very interesting from both a theoretical and practical point of view, they don't influence the derivation and use of the proposed datastructure in it self, but may result in a speed-up of algorithms due to advanced label-checking and verification.**

# A Numerical implementation

**In this section the numerical aspects of the calculation of the points of the symmetry set, its branches and special points, as well as the derivation of the proposed datastructure is given. Since rapid prototyping is done in *Mathematica*$^{TM}$ [40], firstly a short introduction of that computer algebra language/system is given**

## A.1 *Mathematica*

***Mathematica* is a high level interactive mathematical programming language. It consists of two parts: the computing engine called kernel, and a sophisticated user interface. Therefore, the notebook integrates both symbolic and fast numerical capabilities. *Mathematica* is list-oriented, so in contrast to most programming languages, *Mathematica* does not need `for`, `do` or `while` loops to execute commands. As an example, the difference of two equal lengthened lists $p$ and $q$ is simply $p - q$. The matrix containing the difference of two subsequent columns of a matrix $A$ is simply `A - RotateLeft[A]`. This is extremely convenient in image and shape analysis, where are objects can be regarded as lists or listed lists.**

## A.2 Shape parameterization

**If the shape is parameterized, it is straightforward to obtain a discrete version of it. If the shape is given as an implicit function, firstly a pointset is calculated. Note that such sets can also be given as initial set, e.g. as result of a boundary detection algorithm. This pointset is calculated as follows. Given the function $f(x, y) = 0$, a set of values $x_i = x_0 + i\delta x$ is taken, for $x_0$ some initial "most left" value, $\delta x$ a specific stepsize and $i$ ranging from zero to $N$, to reach some "most right" value. Next, for all values $x_i$, in the procedure `Table[Solve[f(x[[i]],y)==0,{y}],{i,1,Length[x]}`, *Mathematica*'s fast analytical functions and list structure is used. This command generates for each $x_i$ a list of values $y_{i_j}$. Of this list, only the real solutions (if they exist) are taken. The result is a list of points $(x_i, y_i)$, $i = 1, \dots M$, where the difference in $x$ values for two subsequent points yields $x_{j+1} - x_j = k\delta x$, for $k \in I\!N$. Next, the same procedure is carried out for the $y$ variable in order to obtain a sampling that is also dense enough at points with a vertical tangent and at small elongated substructures.**

**The second step is ordering the list with points. This is done using the matrix of Euclidian distances between all points. The first point of the list is taken, then the closest point to it (the minimum in the matrix row) is put next to it, the matrix row and column of the first point are filled with maximal values, and so on. The output is a list with the points of the shape in either clockwise or anti-clockwise order (obviously, a small change in the algorithm can force one of the two possibilities). To each point the values of the unit normal are added. They follow either from a direct computation of the implicit function, or, in case of a boundary from a given image, from the derivative, calculated with a Gaussian at a certain scale.**

## A.3 Computation of Symmetry Set Points

**For each two points the (symmetric) matrix $(p_i - p_j).(N_i \pm N_j)$, with $p_i = (x_i, y_i)$ and $N_i = (N_{x_i}, N_{y_i})$, is calculated. Of this matrix the sign is obtained (1,0,-1 for positive, zero or negative, respectively) and the difference for each row with the next row is calculated. If this difference is non-zero, a zero-crossing is traversed. Secondly, anti-symmetry set points are found by applying the same operations to the matrix $(N_{x_i}, N_{y_i}).(-N_{y_j}, N_{x_j})$, being the innerproduct of the normals at $p_i$ and the tangent at $p_j$. The complement of the former set with respect to the latter one yields the zero-crossing points on the shape (the symmetry set points on the pre-symmetry set).**

**The list containing al these point-pairs $(p_i, p_j)$ is then used to compute $p_i - rN_i = p_j - rN_j$ to obtain the distance $r$ from the points on the shape to the symmetry set (i.e. $r$ is the radius of the circle tangent to the two points and the center of the circle is determined by these to equations). Since the equation must hold for both $x$ and $y$ and the zerocrossings are not exact, two values for $r$ are obtained. To avoid this and get one solution, $r$ is obtained as follows. If $p_i - rN_i = p_j - rN_j$, then $(p_i - p_j) = r(N_i - N_j)$ and thus $r = (p_i - p_j)^2/(N_i - N_j).(p_i - p_j)$. Again this does not solve $p_i - rN_i = p_j - rN_j$ exactly. To find the point $SS_k$ of the symmetry set, the average of the two locations $SS_{k_1} = p_i - rN_i$ and $SS_{k_2} = p_j - rN_j$ is taken. This yields a set of points that are part of the symmetry set.**

### A.3.1 Branches, $A_1^2$

**Given de zerocrossings - the pre-symmetry set - the different branches of the symmetry set are obtained by the distinct branches of the pre-symmetry set. It therefore remains to extract the branches in the set of points generated by the zerocrossings algorithm. Since the branches in the pre-symmetry set are closed loops - with respect to a torus representation, i.e. the left and right boundary are connected, as well as the top and bottom, branches of the symmetry set follow directly from the calculated pre-symmetry set. This zerocrossings algorithm, however, yields an unsorted list. So again an Euclidean distance method is used is used to find the nearest neighbour of a point. Generally this neighbour is close, within the eight-neighbourhood of the point. Sometimes there is a hole - due to $A_3$ points or the removal of anti-symmetry set points - and a 24-neighbourhood is needed. If the neighbour is further away and the last found point is close to the starting point, a new branch is started with a new point.**

**All the points that are obtained are initially labeled as $A_1^2$ points, the only non-isolated points on the symmetry set.**

### A.3.2 $A_3$

For each symmetry set branch the begin and endpoint are $A_3$ points. In the pre-symmetry set they are the points with $(p_i, p_i)$. These points, however, are not allowed in the numerical procedures, since they imply multiplications with zero or infinity in the calculation of $r$. So pointsets $(p_i, p_i \pm 1)$ or $(p_i \mp 1, p_i \pm 1)$ are detected. Obviously, only two pointset are taken that are located in the list on a distance of approximately half the listlength to make sure that the two different endpoints are found. The values $p_i$ (or the average of the two positions) of the points are also the ordering of the cusps of the evolute, since the shape is parameterized. The list containing the (pre-) symmetry set contains a list for each branch. They are rotated such that the first element is an $A_3$ point.

### A.3.3 $A_1A_2$, subbranches

At $A_1A_2$ points, the branch in the pre-symmetry set has a horizontal or vertical tangent. So given the list containing the points of the branch in the horizontal and vertical parameter-coordinates, the sign of the difference between subsequent points denotes the sign of the derivative. If plateaus occur, i.e. regions with zeros, they are filled up with the values on the border of the plateau. Taking again the difference between subsequent points (in opposite direction), the non-zero entries denote the zeros of the derivative, that is, the local extrema and thus the $A_1A_2$ points.

Since subbranches have their begin and end points at either $A_3$ points or $A_1A_2$ points, the list of each branch is split up into lists containing the subbranches, beginning and ending at these points.

### A.3.4 $A_1^3$

To find $A_1^3$ points, the minimum Euclidian distance between all possible pairs of triples of symmetry set subbranches are taken. Each pair of subbranches essentially may not be connected by an $A_1A_2$ point. If this distance for each possible pair is less than the original stepsize $\delta x$, the pointlocations are labeled as $A_1^3$. Since their are three minimal distances, at most six, at least three point locations will be found. So on each branch the $A_1^3$ point will be determined by either one or two location. In the latter case, the points are close and either the point in the middle, or one of the points is labeled as $A_1^3$.

### A.3.5 $A_1^2/A_1^2$

A similar procedure as for the $A_1^3$ points can be applied for the $A_1^2/A_1^2$ points. Here only pairs of possible subbranches are compared, where pairs yielding an $A_1^3$ point are ignored. The special $A_1^2/A_1^2$s at infinity are obtained by investigating sign changes of the radius along a symmetry set branch.

## A.4 Results

A notebook in *Mathematica* has been implemented with the algorithms as described above. Most images throughout this deliverable (notable section 4, 6 and 7) are generated with this notebook. A testversion of this notebook will be available at the DSSCV project's website.

As an example of the three different datastructures due to transitions, as described in the example given in section 6, see Figure 25. It shows the output generated by the notebook In each of the three cases the first column gives a pair denoting of a special point both the symmetry set branch and the location along this branch at which it is located. The second column describes the type of the special point and the third column provides extra information on the point: the position in the ordering at $A_3$ points, a label to distinguish identical points in case of $A_1^3$ and $A_1^2/A_1^2$ points, and a label for distinguishing pairs of $A_1A_2$ points. Note that the $A_3$ branches are some times processed in inverse order (the ones with labels 2 and 6), but since the labels determine in which order to go through, this is not harmful.

| | | |
|---|---|---|
| {1, 1} | a3 | 6 |
| {1, 145} | a2a2 | 1 |
| {1, 316} | a3 | 2 |
| {2, 1} | a3 | 4 |
| {2, 117} | a2a2 | 1 |
| {2, 197} | a13 | 1 |
| {2, 202} | a1a2 | 1 |
| {2, 205} | a2a2 | 2 |
| {2, 220} | a1a2 | 1 |
| {2, 233} | a13 | 1 |
| {2, 313} | a3 | 7 |
| {3, 1} | a3 | 9 |
| {3, 48} | a2a2 | 3 |
| {3, 61} | a1a2 | 2 |
| {3, 96} | a1a2 | 2 |
| {3, 114} | a2a2 | 3 |
| {3, 132} | a2a2 | 2 |
| {3, 133} | a13 | 1 |
| {3, 153} | a3 | 10 |

| | | |
|---|---|---|
| {1, 1} | a3 | 2 |
| {1, 189} | a2a2 | 1 |
| {1, 318} | a3 | 6 |
| {2, 1} | a3 | 9 |
| {2, 59} | a2a2 | 2 |
| {2, 74} | a1a2 | 1 |
| {2, 122} | a1a2 | 1 |
| {2, 146} | a2a2 | 2 |
| {2, 194} | a3 | 10 |
| {3, 1} | a3 | 7 |
| {3, 186} | a2a2 | 1 |
| {3, 314} | a3 | 4 |

| | | |
|---|---|---|
| {1, 1} | a3 | 2 |
| {1, 102} | a13 | 1 |
| {1, 115} | a1a2 | 1 |
| {1, 129} | a2a2 | 1 |
| {1, 152} | a1a2 | 1 |
| {1, 167} | a13 | 1 |
| {1, 197} | a2a2 | 2 |
| {1, 318} | a3 | 6 |
| {2, 1} | a3 | 9 |
| {2, 42} | a2a2 | 1 |
| {2, 43} | a13 | 1 |
| {2, 62} | a2a2 | 3 |
| {2, 79} | a1a2 | 2 |
| {2, 136} | a1a2 | 2 |
| {2, 161} | a2a2 | 3 |
| {2, 214} | a3 | 10 |
| {3, 1} | a3 | 7 |
| {3, 180} | a2a2 | 2 |
| {3, 309} | a3 | 4 |

Figure 25: Mathematica$^{TM}$ output: Data representation of the $\mathcal{SS}$ of the oval for $b = 0.09$, $b = 0.015$, and $b = 0.30$.

# B Open questions

**Together with the use of the pre-$\mathcal{SS}$ and the proposed datastructure several questions rise that are mainly theoretical of nature and do not influence the structures itself, but may be used to speed-up algorithms dealing with them.**

- **Concerning the datastructures, it is an open question how significant the difference between the two proposed structures is. If the $A_1A_2$ points in the original structure are augmented with their location on the evolute, the same information is captured as is visualized in the second one.**

- **It is also not clear how complete the structures are: Is all information of the $\mathcal{SS}$ included in the structure? Since the modified structure can be regarded as projecting the evolute and the $\mathcal{SS}$ on a cylinder, by cutting the evolute at one position, and gluing the two parts of the cut together, it appears to be equivalent - at least topological.**

- **It is also not proven that the $\mathcal{SS}$ and the evolute together - let alone the proposed datastructures - are complete. Although it is not likely, is might be that essentially different shapes result in the same structure in pathological cases. However, then the augmented $\mathcal{MA}$ - like the Shock Graph - would suffer from the same problem - which has not been reported.**

- **In the pre-$\mathcal{SS}$ two essential loops are present: These loops are built up by all the points on the shape. One can think of them as the main axes, like for the ellipse. Transitions can introduce closed loops, and transitions can change the structure along loops. It is not a priori clear that certain transitions are forbidden, like the ones acting on two essential loops, changing them into two closed loops and let them both disappear. This would mean that essential loops can be created and annihilated, and one can eventually end up without loops - but this would imply that there is no $\mathcal{SS}$ at all, so the shape has disappeared. There is one lemma stating that each horizontal or vertical line in the pre-$\mathcal{SS}$ should intersect at least two lines,**

**which prohibits the scenario described above. This is a direct consequence from the fact that for a fixed point $p_i$ probing all other points $p_j$ yields a $2\pi$ rotation of the difference vector, while the sum of normals yields also a $2\pi$ rotation, but in the opposite direction. So there are at least two zerocrossings.**

**The general situation at which a transition can occur, is probably sufficient to make clear which outcomes are possible, e.g. the presence of several lines of the evolute, assuming in general at least four cusp points of the evolute, i.e. at least four $A_3$ points and thus at least two $\mathcal{SS}$ branches (essential loops).**

- **So there are at least two essential loops, but can there be more? The answer may be no, but is at least "even", since extra branches of the $\mathcal{SS}$ can only be created by selfintersections of the evolute. These events cause the swallowtailbranches (closed loops), that then should grow out to be global branches (essential loops). Two pairs in the pre-$\mathcal{SS}$ are then "banana"-shaped, symmetric in the anti-diagonal, and grow together at the boundaries ('in the middle'), where they exchange an branch.**

- **Another interesting event is the occurence of closed loops in closed loops: there is no reason why they could not occur: it corresponds to a swallowtail in a swallowtail of the evolute.**

- **Furthermore, the datastructures bear relations that are also present in the pre-$\mathcal{SS}$. Since the $A_3$ points relate to consecutive maxima and minima of the curvature, these maxima and minima relate to even and odd labels in the structure.**

- **A closed loop in the pre-$\mathcal{SS}$ links a maximum and a minimum - and thus a even and odd label. In the "creation of two essential loops" as described above, two closed loops - two times a minimum and a maximum, two times a combination of an odd and an even label - change into two essential loops - a minimum pair and a maximum pair, an odd pair and an even pair. In the enclosed closed loop situation, it is simply minimum - maximum - minimum - maximum, or odd - even - odd - even.**

- **Suppose that a closed component $C$ of the pre–$\mathcal{SS}$ represents the element $(a, b)$ in the integer homology of the torus; this means that, in an oriented sense, $C$ winds $+a$ times round 'left to right' and $+b$ times 'top to bottom'. There is a general rule that an $(a, b)$ curve and a $(c, d)$ curve on the torus have intersection number $ad - bc$ so long as each intersection is transverse. Each transverse intersection is given a sign, $\pm 1$, according to whether the rotation from one oriented tangent to the other agrees with or does not agree with the orientation of the torus, and these add to $ad - bc$.**

  **Now the "reflexion" of $C$ in the diagonal will either be $C$ itself, in which case clearly $a = b$, or it will be another component $C'$ of the pre–$\mathcal{SS}$, of type $(b, a)$. In the latter case the intersection number is $a^2 - b^2$ and the only way this can be $0$ ($C$ and $C'$ are disjoint) is $a = \pm b$. So in all cases $a = \pm b$, and to avoid self-intersections we must therefore have $(a, b) = (0, 0), (1, 1), (1, -1)$. [$(-1, 1)$ and $(-1, -1)$ are the same as these but orienting $C$ the other way.]**

  **So every component of the pre–$\mathcal{SS}$ has one of these 'winding numbers' on the torus. Note that the diagonal has $(1, 1)$. We can go on to examine the way in which the transitions (moth, nib etc.) affect the number of components with these different $(a, b)$. In fact the only ones which have any effect are the moth, nib and $A_4$ transitions. The moth alters $\#(0, 0)$ by 2 (and adds no diagonal points), the $A_4$ alters $(0, 0)$ by 1 and alters the number of diagonal points by 2. What about the nib? Can we look at cases to decide the effect of this transition on $\#(1, -1)$ etc? If so it might be possible to say something about the pre–$\mathcal{SS}$ of a general curve, starting from the ellipsee which has $\#(1, -1) = 2$.**

- **Finally, it remains if the ellipse is "the mother of all shapes", in the sense that all other shapes can be obtained by modifying it. The dual formulation would be that the $\mathcal{SS}$ containing only two branches is "the father of all $\mathcal{SS}$s", from which all other $\mathcal{SS}$s can be obtained by applying subsequent transitions. The same holds of course for the pre-$\mathcal{SS}$ containing only two essential loops, adding closed loops and local extrema (the $A_1A_2$'s).**

## References


[1] DSSCV meeting at the Isle of Skye, Scotland, UK, June, 2003.

[2] T.F. Banchoff and P. J. Giblin. Global theorems for symmetry sets of smooth curves and polygons in the plane. *Proceedings of the Royal Society of Edinburgh*, 106(A):221–231, 1987.

[3] A. Belyaev and S. Yoshizawa. On evolute cusps and skeleton bifurcations. In *Shape Modeling and Applications, SMI 2001 International Conference on.*, pages 134–140. IEEE Computer Society, 2001.

[4] S Betelu, G Sapiro, A Tannenbaum, and P Giblin. Noise-resistant affine skeletons of planar curves. In *Proceedings of the 6th European Conference on Computer Vision (2000)*, volume 1842, pages 742–754, 2000. LNCS 1842.

[5] A. Blake and M. Taylor. Planning planar grasps of smooth contours. *Robotics and Automation, 1993. Proceedings., 1993 IEEE International Conference on*, pages 834–839 vol.2, 1993.

[6] A. Blake, M. Taylor, and A. Cox. Grasping visual symmetry. *Computer Vision, 1993. Proceedings., Fourth International Conference on*, pages 724–733, 1993.

[7] S Bouix and K Siddiqi. Divergence-based medial surfaces. In *Proceedings of the 6th European Conference on Computer Vision (2000)*, volume 1842, pages 603–620, 2000. LNCS 1842.

[8] J. W. Bruce and P. J. Giblin. *Curves and Singularities*. Cambridge University Press, 1984.

[9] J. W. Bruce and P. J. Giblin. Growth, motion and 1-parameter families of symmetry sets. *Proceedings of the Royal Society of Edinburgh*, 104(A):179–204, 1986.

[10] J. W. Bruce, P. J. Giblin, and C. Gibson. Symmetry sets. *Proceedings of the Royal Society of Edinburgh*, 101(A):163–186, 1985.

[11] P. Dimitrov, J.N. Damon, and K. Siddiqi. Flux invariants for shape. *Computer Vision and Pattern Recognition, 2003. Proceedings. IEEE Conference on*, 1:x–x vol.1, 2003.

[12] P. Dimitrov, C. Phillips, and K. Siddiqi. Robust and efficient skeletal graphs. *Computer Vision and Pattern Recognition, 2000. Proceedings. IEEE Conference on*, 1:417–423 vol.1, 2000.

[13] P. J. Giblin and B. B. Kimia. On the intrinsic reconstruction of shape from its symmetries. In *IEEE Conference on Computer Vision and Pattern Recognition, 1999*, pages 79–84, 1999.

[14] P. J. Giblin and B. B. Kimia. On the local form and transitions of symmetry sets, medial axes, and shocks. In *Proceedings of the 7th International Conference on Computer Vision (1999)*, pages 385–391, 1999.

[15] P. J. Giblin and B. B. Kimia. On the intrinsic reconstruction of shape from its symmetries. *IEEE Transactions on Pattern Analysis and Machine Intelligence*, 25(7):895–911, July 2003.

[16] P. J. Giblin and B. B. Kimia. On the local form and transitions of symmetry sets, medial axes, and shocks. *International Journal of Computer Vision*, 54(1/2):143–156, 2003.

[17] Peter J Giblin and Guillermo Sapiro. Affine-invariant distances, envelopes and symmetry sets. *Geometriae Dedicata*, 71(3):237–262, 1998.

[18] P.J. Giblin. 2D symmetry sets; graphical representation. Handout containing a summary and consequences of discussion at [1].

[19] P.J. Giblin and G. Sapiro. Affine invariant medial axis and skew symmetry. *Computer Vision, 1998. Sixth International Conference on*, pages 833–838, 1998.

[20] J. Gomes and O. Faugeras. Reconciling distance functions and level sets. *Scale-Space Theories in Computer Vision. Second International Conference, Scale-Space '99. Proceedings (Lecture Notes in Computer Science Vol.1682)*, pages 70–81, 1999. identical to Journal of Visual Communication and Image Representation, 11:2, 209-23, 2000, and Level Sets and Distance Functions, ECCV 2000, LNCS 1842, 588-602.

[21] M. Hisada, A. G. Belyaev, and T. L. Kunii. Towards a singularity-based shape language: ridges, ravines, and skeletons for polygonal surfaces. *Soft Computing*, 7(1):45–52, 2002.

[22] P. A. Holtom. *Affine-Invariant Symmetry Sets*. PhD thesis, University of Liverpool, 2000.

[23] S. N. Kalitzin, B. M. ter Haar Romeny, A. H. Salden, P. F. M. Nacken, and M. A. Viergever. Topological numbers and singularities in scalar images. Scale-space evolution properties. *Journal of Mathematical Imaging and Vision*, 9(3):253–296, November 1998.

[24] T.L. Kunii, A.G. Belyaev, E.V. Anoshkina, S. Takahashi, R. Huang, and O.G. Okunev. Hierarchic shape description via singularity and multiscaling. In *Computer Software and Applications Conference, 1994. COMPSAC 94. Proceedings., Eighteenth Annual International*, pages 242–251. IEEE Comput. Soc. Press, 1994.

[25] S. Osher and N. Paragios, editors. *Geometric Level Set Methods in Imaging, Vision, and Graphics*. Springer, 2003.

[26] M. Pelillo, K. Siddiqi, and S. Zucker. Matching hierarchical structures using association graphs. *IEEE Transactions on Pattern Analysis and Machine Intelligence*, 21(11):1105–1120, 1999.

[27] H. Rom and G. Medioni. Hierarchical decomposition and axial shape description. *IEEE Transactions on Pattern Analysis and Machine Intelligence*, 15(10):973–981, 1993.

[28] T.B. Sebastian, P.N. Klein, and B. B. Kimia. Recognition of shapes by editing shock graphs. In *Proceedings of the 8th International Conference on Computer Vision (2001)*, pages 755–762, 2001.

[29] T.B. Sebastian, P.N. Klein, and B. B. Kimia. shock-based indexing into large shape databases. In *Proceedings of the 7th European Conference on Computer Vision (Copenhagen, Denmark, May 28–31, 2002), LNCS 2352*, pages 731–746, 2002.

[30] J. A. Sethian. Fast marching methods. *SIAM Review*, 41(2):199–235, 1999.

[31] K. Siddiqi, S. Bouix, A. Tannenbaum, and S. W. Zucker. The Hamilton-Jacobi skeleton. In *Proceedings of the 78th International Conference on Computer Vision (1999)*, pages 828–834, 1999.

[32] K. Siddiqi, B. B. Kimia, A. Tannenbaum, and S. W. Zucker. Shapes, shocks and wiggles. *Image and Vision Computing*, 17:365–373, 1999.

[33] K. Siddiqi and B.B. Kimia. A shock grammar for recognition. *Computer Vision and Pattern Recognition, 1996. Proceedings CVPR '96, 1996 IEEE Computer Society Conference on*, pages 507–513, 1996.

[34] K. Siddiqi, A. Shokoufandeh, S. Dickinson, and S. Zucker. Shock graphs and shape matching. *International Journal of Computer Vision*, 30:1–22, 1999.

[35] K. Siddiqi, A. Tannenbaum, and S.W. Zucker. A hamiltonian approach to the eikonal equation. In E.R. Hancock and M. Pelillo, editors, *Energy Minimization Methods in Computer Vision and Pattern Recognition. Second International Workshop, EMMCVPR'99. Proceedings (Lecture Notes in Computer Science Vol.1654)*, pages 1–13. Springer-Verlag, 1999.

[36] Kaleem Siddiqi, Sylvain Bouix, Allen Tannenbaum, and Steven W. Zucker. Hamilton-jacobi skeletons. *International Journal of Computer Vision*, 48(3):215–231, 2002.

[37] H. Tek and B.B. Kimia. Perceptual organization via the symmetry map and symmetry transforms. *Proceedings. 1999 IEEE Computer Society Conference on Computer Vision and Pattern Recognition (Cat. No PR00149)*, pages 471–7 Vol. 2, 1999.

[38] Huseyin Tek and B.B. Kimia. Symmetry maps of free-form curve segments via wave propagation. *Computer Vision, 1999. The Proceedings of the Seventh IEEE International Conference on*, 1:362 –369 vol.1, 1999.

[39] Huseyin Tek and Benjamin B. Kimia. Boundary smoothing via symmetry transforms. *Journal of Mathematical Imaging and Vision*, 14(3):211–223, 2001.

[40] S. Wolfram, editor. *The Mathematica Book*. Wolfram Media / Cambridge University Press, Cambridge, fourth edition, 2000. See also http://www.wolfram.com.